NTNU

Norwegian University of
Science and Technology

Torsion Buckling of Dynamic Flexible Risers

Evgenii Koloshkin

Marine Technology
Submission date: June 2016
Supervisor: Svein Sævik, IMT

Norwegian University of Science and Technology
Department of Marine Technology

NTNU – Trondheim
Norwegian University of
Science and Technology

Torsion Buckling of Dynamic Flexible Risers

Evgenii Koloshkin

June 2016

MASTER THESIS

Department of Marine Technology

Faculty of Engineering Science and Technology

Norwegian University of Science and Technology

Supervisor: Prof. Svein Sævik

Summary

The main purpose of this work is to contribute to better understanding of the torsion structural stability and kink formation process of flexible risers in catenary configuration.

The thesis deals with installation criteria of offshore flexible lines (risers/cables) with focus on the torsion buckling behavior at the touch down point. The study includes both analytical and numerical investigations. The latter is carried out by means of the non-linear finite element program BFLEX2010.

The physical nature of the torsion buckling of catenary risers has been thoroughly analyzed and described in the present work for the models with linear and non-linear material characteristics. It has been found that it is important to include the riser's section resting on the seabed to the models because it is subjected to friction forces influencing torsion buckling capacity.

The numerical performance of the models obtained by BFLEX2010 software has been compared to the analytical solution represented by the Greenhill's equation. The limitation of the Greenhill's equation with respect to the torsion buckling at the TDP has been evaluated.

Significant efforts have been dedicated to investigation of the effect of non-linear moment curvature behavior (the sliding process between riser's layers) on the process of torsion buckling. It has been found that the torsion buckling capacity is directly proportional to the value of the friction moment.

The effect of cyclic heave motion of the laying vessel on kink formation process has also been studied at different levels of initial utilization of torsion reaction. Parametric numerical analysis showed that in some cases depending on heave amplitude and amount of initial torsion utilization there can be a severe consequences leading to kink formation. Therefore, the methodology called "Dynamic criterion" has been established for evaluation of the kink formation process and verified for the models with linearly elastic and non-linear material properties. Another important observation has been done from the cyclic heave motion analysis that the structure at the same time can have a compression in the TDP and remain safe against torsion failure modes. This conclusion challenges current offshore industry practice.

Preface

This report is the outcome of the Master's thesis work in marine structural mechanics at the Department of Marine Technology, NTNU. The thesis has been carried out during the spring semester 2016 and it represents a logical continuation of the specialization project performed in the fall of 2015.

It should be noted that some changes have been made in the list of content and the title of the thesis with approval from the supervisor.

The major and most difficult part of the project was analysis of the torsion buckling of flexible risers under various conditions by means of the computer program BFLEX2010. Significant amount of time was spent on understanding of non-linear finite element theory that stands behind the software. It was a great feeling when I realized that I can use the BFLEX2010 not as a "black box" but as a powerful tool for achieving my thesis objectives.

I am also very satisfied that I could manage to develop MATLAB scrips that can interpret/sort out/manipulate data from the BFLEX2010 output files and generate multiple plots automatically.

I do appreciate the fact that I had the chance to approach the torsion buckling problem analytically. Deriving analytical expressions enabled me to get deep down to the nature of the physical process and to use obtained equations for verification of the BFLEX2010 results.

I would like to express a sincere gratitude to my supervisor, Prof. Svein Sævik for the help and guidance he has provided during the work on this thesis. His professional knowledge in the field of structural mechanics, kindness and good sense of humor made the experience of working with him unforgettable.

I dedicate this thesis to my family, especially to my mother. Without her constant mental support and encouragement my two-year staying in Norway would be impossible.

Trondheim, June 6th, 2016

Evgenii Koloshkin

Scope of work

The thesis is organized in a rational manner to give a clear exposition of results, assessments, and conclusions. The work contains following elements: Summary, preface, scope of work, list of contents, main body of thesis, conclusions with recommendations for further work, list of symbols and abbreviations, references and appendices. All figures, tables and equations are numerated. Scope of work is represented below:

1. Literature study including flexible pipe technology, failure modes and design criteria with particular focus on the local tensile armour buckling failure mode, analytical methods for buckling analysis of flexible pipes and the non-linear Marintek FE software Bflex2010.

2. Establish a global FEM model in Bflex for analyzing the global torsion buckling failure mode during installation. This is to include two models: One based on elastic properties with reference to the one published by Neto and Martins, 2013, one model that includes the non-linear moment-curvature behavior

3. Demonstrate the performance of the two models

4. Compare the results with results from analytical equations

5. Investigate the effect of cyclic heave motion of the vessel on kink formation process.

6. Conclusions and recommendations for further work

List of applied computer programs

Following computer programs were used during the work on the thesis:

Bflex2010 [1] The thesis is based on this program. It was utilized for non-linear FEM modeling and analysis.

Bflex2010post [2] Bflex2010 post processing (export of the results from Bflex2010 output *.raf* files).

Matlab [3] The software was used for carrying out all computational operations. The MATLAB scripts were also developed for reading/manipulation the data from the BFLEX2010POST output files and automatic generation of multiple plots.

Cygwin It was applied for operations with Bflex2010 input files and generation/execution of multiple analyses.

Xpost Graphical interpretation of the results from Bflex2010 output *.raf* file.

Matrixplot Building plots based on ASCII files generated by Bflex2010post.

Latex The report was written and compiled by this program.

[1] The Bflex2010 input files for all models described in the thesis are provived in the Digital Attachment enclosed to the thesis. One example of the Bflex2010 input file for the simplified beam model is shown in the Appendix A.1.

[2] The example of the Bflex2010post input file can be found in the Appendix A.2.

[3] Appendix B demonstrates the example of MATLAB script for reading output data and plot generation.

Nomenclature

Roman letters

a_0	Heave amplitude
$a(t)$	Heave motion
A_i, $i = 1,2$	Constants from the differential equilibrium equation
B_i, $i = 1,2$	Constants from the differential equilibrium equation
C	Elasticity (constitutive) matrix
d	Water depth
d_e	External riser diameter
dr	Displacement increment
dR	Load increment
E	Young's modulus
EA	Axial stiffness
EI	Bending stiffness
EI_e	Linearly elastic bending stiffness
EI_i	Initial stiffness
f_i, $i = x, y, z$	Unit soil resistance in i-direction
F	Volume forces
GI	Torsion stiffness
i_i^a, i_i^b	Orthonormal base vector triads
j_i	Element reference system
K_0	Linear (initial) stiffness
K_I	Incremental (tangent) stiffness
K_g	Geometric stiffness
l	Beam length
M_{cr}^0	Critical reaction torsion moment for buckling without axial force
M_f	Friction moment
M_t	Torsion moment

M_{ty}	Bending component in y-direction
M_{tz}	Bending component in z-direction
M_x	Reaction torsion moment
M_x^{crit}	Critical reaction torsion moment or torsion buckling moment
n	Iteration number
P	Compressive force
P_{cr}^0	Critical compressive axial force for buckling without torsion moment
R_{ext}	External load
R_{int}	Internal load
S	Catenary length
T	Tensile load
T_0	Horizontal bottom tension
T_h	Heave period
u	Displacement vector
$v(x)$	Displacement in y-direction
$w(x)$	Displacement in z-direction
w_s	Submerged weight

Greek letters

α	Riser top angle
$\tilde{\alpha}$	Tensile wire lay angle
β	Tension/torsion coupling parameter
δr	Displacement vector change
Δ	Differential matrix operator
ε	Strain vector
ε_0	Initial strain vector
ε_s	Tensile armor strain
ε_x	Center line strain
θ_x	Prescribed axial rotation about x-axis
κ_{CG}	Closed gaps curvature
κ_{crit}	Critical curvature
$\kappa_i,\ i = y,z$	Curvature about i-axis
κ_t	Total curvature
κ_{t-max}	Maximum value of total curvature
$\mu_i,\ i = x,y$	Coulomb friction coefficient in i-direction
σ	Internal stress
τ	Torsion

Abbreviations

PSA	The Petroleum Safety Authority Norway
NCS	Norwegian Continental Shelf
TDP	Touch Down Point
TDZ	Touch Down Zone
FEM	Finite Element Method
CTL	Corotated Total Lagrangian formulation
BC	Boundary Condition
DOF	Degrees of Freedom

List of Figures

List of Tables

Contents

Chapter 1

Flexible riser technology

1.1 Introduction

Flexible risers are widely used in the offshore production of oil and gas. According to (API17B [2]) flexible riser is a flexible pipe which is a connection between a platform/ship/etc. and a flowline/seafloor installation/another platform where the riser can take freely suspended (free, catenary)/restrained to some extent (buoys, chains)/ totally restrained or enclosed in a tube forms.

The first introduction of flexible risers in offshore industry happened in the beginning of 70's and first installation occurred in 1976 on Petrobras Garoupa. Another important fact is that in 1983/84 the technology appeared for dynamic flexible risers in the harsh environment condition of the North Sea. (Berge et al. [7]). Over the years a tremendous research programs have been launched in that sphere and many important achievements have been reached regarding design philosophy, however there are still a lot of intricate challenges remain unquestioned. In (4SubseaAS [1]) report for The Petroleum Safety Authority Norway (PSA) it is stated that PSA Norway considers "...flexible risers is an area where the industry still has a clear and pressing potential for improvement". Important to mention that there has been a substantial leap in the number of flexible risers on the Norwegian Continental Shelf (NCS) over the last 30 years and it can be seen in the Figure 1.1.

Finishing introduction it is worth to note why flexible risers are more preferable than rigid steel pipes (Berge et al. [7]):

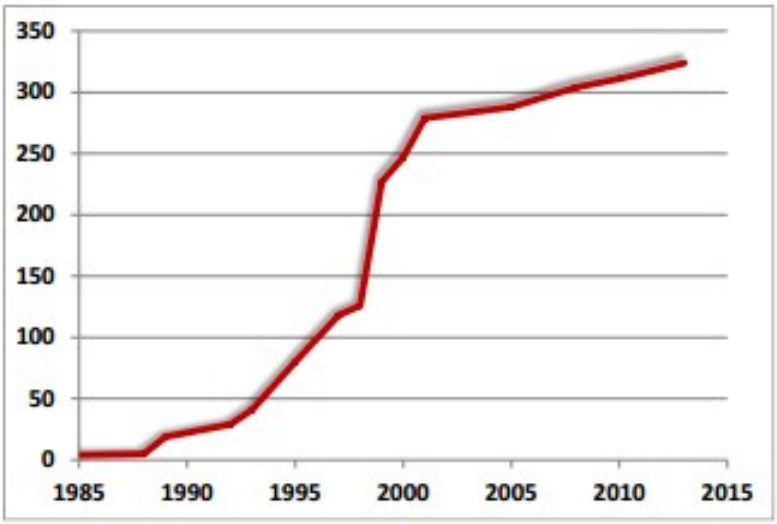

Figure 1.1: Accumulated number of installed flexible risers (4SubseaAS [1])

- Flexible pipes can perform efficiently permanent connections between floaters with large motions and subsea installations
- Simplified way of transportation and installation

1.2 Riser configuration design

There are many different riser system configurations and a selection process for configuration design is based on the following factors (Bai [4]),(Berge et al. [7]):

- Costs
- Material
- Physics of environment
- Depth of water
- Geometry and global behavior
- Number of risers
- Means of support

The most cost-effective and simplest configuration for deep and environmentally moderate waters is a free hanging catenary because it does not require advanced subsea infrastructure and installation process is relatively simple. This method found its popularity in Brazilian offshore industry. While in the North Sea there is a need for configurations with additional flexibility like lazy/steep wave or lazy/steep S due to a harsh environment conditions. These design solutions with additional buoyancy will allow larger floater motions and substantially reduce the top tension and the touch down point (TDP) loads (Berge et al. [7]). All these configurations are represented in the Figure 1.2.

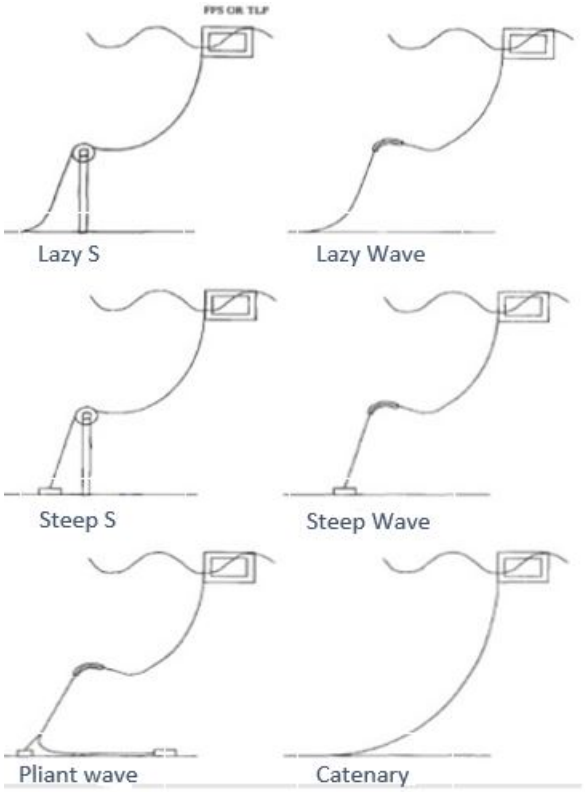

Figure 1.2: Riser configurations (Bai [4])

1.3 Main global strength characteristics and pipe wall structure

There are two generic types of flexible risers depending on cross section structure. First one is a bonded flexible riser which has a reinforcement within surrounding rubber. Second type is a non-bonded flexible riser, which nowadays is more widely used. The present work is focused

on this type. The name “non-bonded” comes from the ability of each structural layer to slide relatively to neighboring layers (with consideration of friction) (Sævik [19]).

Flexible riser concept has proved its effectiveness over the years due to global strength characteristics listed below (Berge et al. [7]):

- Low bending stiffness
- High pressure resistance due to large volume stiffness and strength
- High capacity with regard to axial tensile loading
- Low axial compressive stiffness and strength
- Small torsion resistance

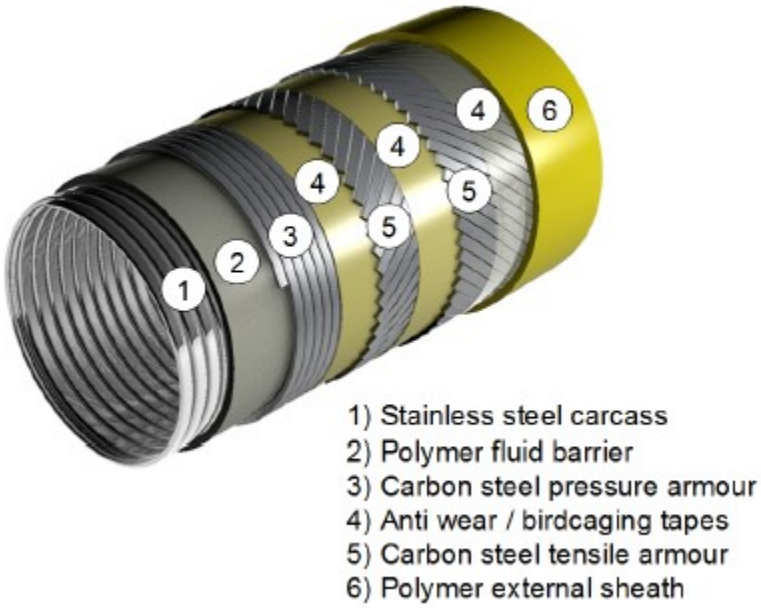

Figure 1.3: Typical non-bonded flexible riser cross section (Berge et al. [7])

Desired strength characteristics of the flexible risers can be achieved by creating a composite wall structure with multiple layers. Each layer performs its unique role. Basically, the structural components can be divided into two types: sealing layers maintaining containment of the transported product and armor reinforcements providing structural strength and integrity. Typical cross section of non-bonded flexible riser is showed in the Figure 1.3 and function of each layer presented in the Table 1.1.

Layer (Berge et al. [7])	Function (Berge et al. [7])
Carcass is a non-hermetic interlocked metallic profile supporting inner liner and contacting with transporting fluid	• External hydrostatic pressure resistance • Crushing loads resistance • Protection of inner liner during pigging operation
Inner liner is a thermoplastic sealing layer	Fluid containment and transportation without leakages
Pressure armor is Zeta, C-clip or Theta interlocked spiral profile	• Hoop stress resistance • Liner's support • Crushing loads resistance
Tensile armor is a two or four layers of helically counter-wound steel wires with a lay angle of between 30 and 35 deg	• Axial capacity • Torsion resistance
Anti-wear tape is no leak-proof thermoplastic tape with thickness of around 1 mm which is utilized between steel armor layers	• Contact stress capacity • Wear and fretting fatigue prevention
Anti-buckling tape is aramid or glass fiber reinforced which is utilized on the outer tensile armor layer	• 'Birdcaging' prevention • Lateral buckling prevention
Outer sheath is a thermoplastic sealing layer	• Sealing against sea water (external fluid barrier) • Impact, erosion and tearing resistance

Table 1.1: Flexible riser layers and their functions

1.4 Physical behavior of unbonded flexible risers

The most crucial aspect of the physical behavior of flexible risers is the nature of risers flexibility. The main question is why such a rigid, high complexity and multi-layered structure as unbonded riser can perform flexible behavior. Considering bending load for relatively small moments, flexible riser will be as rigid as a steel pipe of same dimensions. However, moment can be increased gradually until the level called **the friction moment** M_f, when there will be

a substantial drop in bending stiffness. (Sævik [17]) Since then, riser demonstrates a flexible behavior. This can be observed in the Figure 4 depicting non-linear moment curvature relationship. Before the friction moment level there is no slip between tensile armor layers and supporting pipe structure due to friction forces, which prevent sliding of tensile layers. The second region of the graph starts from the friction moment when slip and dramatic reduction of bending stiffness take place. This region is governed by the new bending stiffness called **the sliding bending stiffness**, which depends on the stiffness of plastic layers, local torsion and bending in each tensile tendon. (Sævik [17]) The third region of the Figure 1.4 starts when there is no space any more between tensile tendons. Initial gaps between them are closed, which is characterized by **the closed gaps curvature** κ_{CG}.

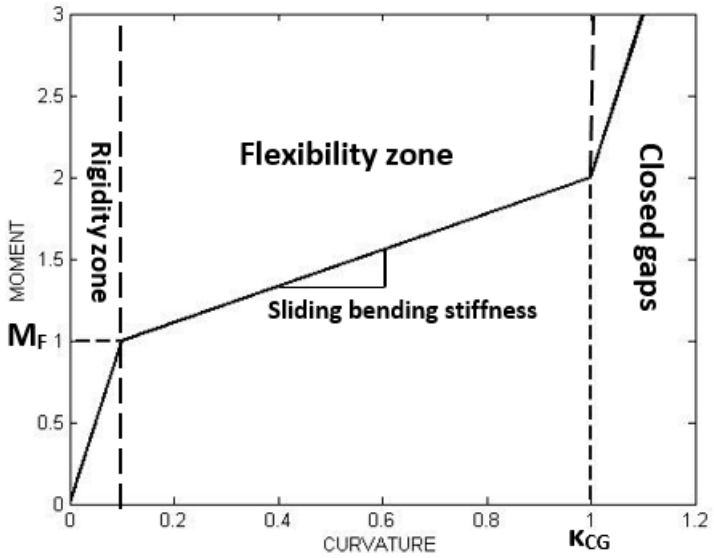

Figure 1.4: Behavior in bending (Sævik [17])

Chapter 2

Failure modes and design criteria

2.1 Introduction

Flexible riser is a very complex composite structure that consists of different layers and each layer has many possible failure modes. Failure in one layer can cause a serious issues for the whole structure. Due to these facts flexible riser can be considered as a complicated machine or mechanical system. Therefore, there is a need to pay significant attention to failure modes assessment. In addition, according to information from PSA Norway, the total number and significance of flexible risers incidents have been increased. It has been even more frequent than for steel risers and pipeline incidents. (4SubseaAS [1]). Increasing trend of flexible riser incidents provided by PSA Norway is depicted in the Figure 2.1.

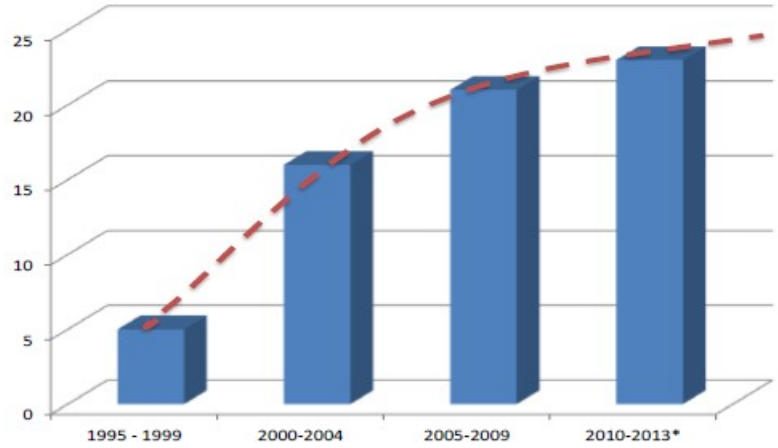

Figure 2.1: Flexible riser incidents (4SubseaAS [1])

2.2 Failure modes

Before discussion of different failure modes it is important to identify what is meant by loss of functionality of flexible riser caused by a certain ultimate failure. This is presented in the Figure 2.2 which was created based on information from (Berge et al. [7]).

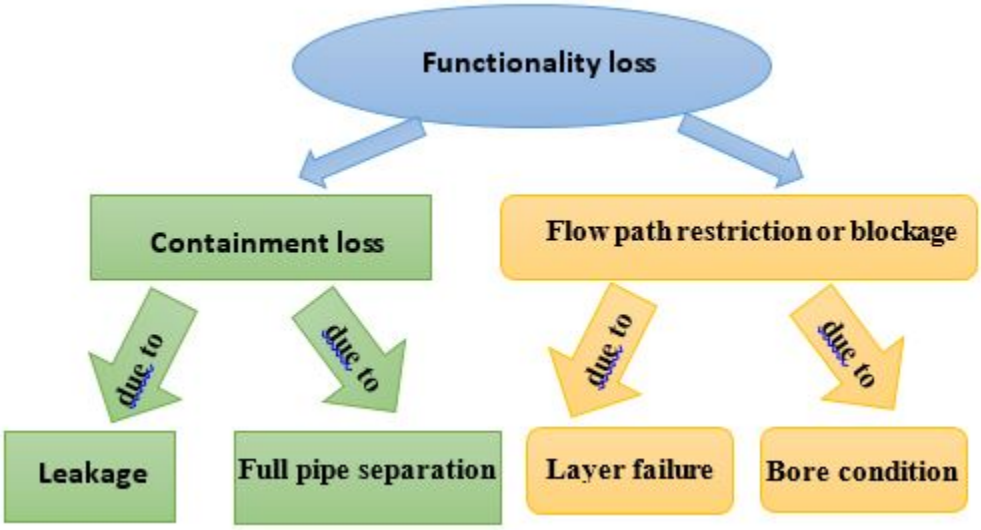

Figure 2.2: Functionality loss

Over the recent years it was reported by PSA Norway that there has been at least 1.5 % probability of failure per riser per operational year. (4SubseaAS [1]) Therefore, it is necessary to take into consideration all possible failure modes during design process. This is important because a certain failure mode can cause a layer failure with associated loss of functionality. Consequently, a subsequent failure of other layers can be triggered ending up in a functionality loss of the whole structure. API Recommended Practice 17B (API17B [2]) provides detailed description of various failure mechanisms and corresponding remedies for flexible pipes that have to be used in order to prevent a certain failure mode. This is shown in the Table 2.1 (API17B [2]).

Tension, compression, torsion, collapse and fatigue are the most critical failure modes, especially for a harsh Norwegian metocean conditions. The present work focuses on detailed analysis of torsion failure mode and on the physics of its severe consequences such as kink formation process.

Potential Failure Mechanisms	Remedies
Collapse Failure Mode	
1. Collapse of carcass and/or pressure armor due to excessive tension. 2. Collapse of carcass and/or pressure armors due to excess external pressure. 3. Collapse of carcass and/or pressure armor due to installation loads or ovalization due to installation loads. 4. Collapse of internal pressure sheath in smooth bore pipe.	1. Increase thickness of carcass strip, pressure armor or internal pressure sheath (smooth bore collapse). 2. Modify configuration or installation design to reduce loads. 3. Add intermediate leak-proof sheath (smooth bore pipes). 4. Increase the area moment of inertia of carcass or pressure armour
Burst Failure Mode	
1. Rupture of pressure armors because of excess internal pressure. 2. Rupture of tensile armors due to excess internal pressure.	1. Modify design, e.g., change lay angle, wire shape, etc. 2. Increase wire thickness or select higher strength material if feasible. 3. Add additional pressure or tensile armor layers
Tension Failure Mode	
1. Rupture of tensile armors due to excess tension. 2. Collapse of carcass and/or pressure armors and/or internal pressure sheath due to excess tension. 3. Snagging by fishing trawl board or anchor, causing overbending or tensile failure.	1. Increase wire thickness or select higher strength material if feasible. 2. Modify configuration designs to reduce loads. 3. Add two more armor layers. 4. Bury pipe
Compression Failure Mode	
1. Birdcaging of tensile armor wires. 2. Compression leading to upheaval buckling and excess bending.	1. Avoid riser configurations that cause excessive pipe compression. 2. Provide additional support/restraint for tensile armors, such as tape and/or additional or thicker outer sheath.
Overbending Failure Mode	
1. Collapse of carcass and/or pressure armor or internal pressure sheath. 2. Rupture of internal pressure sheath. 3. Unlocking of interlocked pressure or tensile armour layer. 4. Crack in outer sheath.	1. Modify configuration designs to reduce loads.
Torsion Failure Mode	
1. Failure of tensile armor wires. 2. Collapse of carcass and/or internal pressure sheath. 3. Birdcaging of tensile armor wires.	1. Modify system design to reduce torsion loads. 2. Modify cross-section design to increase torsion capacity.
Fatigue Failure Mode	
1. Tensile armour wire fatigue. 2. Pressure armour wire fatigue.	1. Increase wire thickness or select alternative material, so that fatigue stresses are compatible with service life requirements. 2. Modify design to reduce fatigue loads.
Erosion Failure Mode	
1. Of internal carcass.	1. Material selection. 2. Increase thickness of carcass. 3. Reduce sand content. 4. Increase MBR.
Corrosion Failure Mode	
1. Of internal carcass. 2. Of pressure or tensile armor exposed to seawater, if applicable. 3. Of pressure or tensile armor exposed to diffused product.	1. Material selection. 2. Cathodic protection system design. 3. Increase layer thickness. 4. Add coatings or lubricants

Table 2.1: Check list of failure modes for primary structural design of unbonded flexible pipe (API17B [2])

2.3 Local tensile armor failure modes

Special approach has to be considered against local tensile armor failure modes at the TDP region, which can bring many troubles during installation process. Bending loads plus large external pressure load at the TDP causing high true wall compression can initiate several local buckling scenarios of tensile wires. Regarding the focus of the present work, one of the consequences of local tensile failure mode is that unfailed tensile layers can get into torsion unbalanced condition inducing axial rotation of the structure. In the most critical case riser can be turned into a kink.

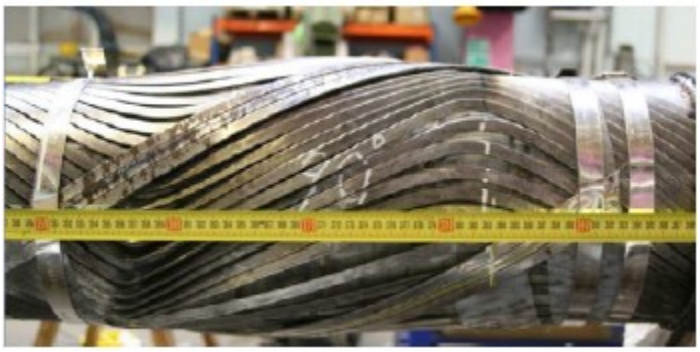

Figure 2.3: Severe lateral buckling behavior (Østergaard et al. [14])

There are two major types of local failure modes leading to the functionality loss of tensile armor, which are local lateral and radial buckling.

Lateral buckling

Lateral buckling occurs at transversely unstable condition below the high-strength tape when radial deflection is sufficiently restrained. This failure mode is considered to be much more complicated with comparison to another buckling type – a radial buckling. The main reason for that is challenges for a lateral buckling detection. It cannot be identified without precise measurements, while a radial buckling can be detected by visual inspection methods (Østergaard et al. [15]). There are some possible remedies to lateral buckling failure mode: increasing of wire and outer sheath dimensions. (Berge et al. [7]). The example of lateral buckling behavior is taken from (Østergaard et al. [14]) and provided in the Figure 2.3.

Radial buckling

Radial buckling, known as birdcaging, occurs at radially unstable condition when tensile wires cannot resist compressive loads any longer and start to deflect in radial direction, which eventually resembles shape of a bird cage (Østergaard et al. [15]). Birdcaging can be also triggered by torsion if load is applied in unwinding direction of the outer tensile armor layer. In order to prevent radial buckling, anti-birdcaging tape may be implemented (Berge et al. [7]). The example of radial buckling behavior is taken from (Østergaard et al. [15]) and showed in the Figure 2.4.

Figure 2.4: Radial buckling behavior (Østergaard et al. [15])

2.4 Design criteria

Flexible risers have to be designed to meet all safety requirements under different loadings. According to (API17J [3]) loads are classified into 3 major groups:

- *Functional loads* – including dead weight, internal and external pressure
- *Environmental loads* – including effects from wind wave and current
- *Accidental loads* – can be caused by various accidents (e.g. collisions, falling objects)

These loads consist of many different subclasses, which can be found in Table 5 in (API17J [3]). The main idea of design philosophy is that flexible riser should satisfy all necessary require-

ments under various combinations of load subclasses. (API17J [3]) and (API17B [2]) are main sources for flexible riser design criteria. In (API17J [3]) design criteria are provided in the form of utilization factors which represent ratio between load and structural resistance. Utilization factors for different structural layers can be used from Table 6 in (API17J [3]). For instance, utilization factor for tensile armor should be taken as 0.67 for normal recurrent operation with functional and environmental loads. Detailed description is provided in (API17B [2]) for following design aspects:

- Strain (polymer sheath).
- Creep (internal pressure sheath).
- Stress (metallic layers and end fitting).
- Hydrostatic collapse (buckling load).
- Mechanical collapse (stress induced from armor layers).
- Torsion.
- Crushing collapse and ovalisation (during installation).
- Compression (axial and effective).
- Service life factors.

Chapter 3

Theory and analytical methods

3.1 Finite Element Method

The present thesis broadly deals with a practical use of the Finite Element Method (FEM) in the structural analysis. Therefore, main hallmarks of the FME are briefly discussed in this chapter.

Various physical phenomena in structural mechanics can be expressed by the following fundamental differential equations (Bell [6]):

- *Equilibrium* between external loads and internal stresses

$$\Delta^T \cdot \sigma + F = 0 \tag{3.1}$$

where σ stands for internal stress components and F for volume forces. The matrix operator Δ is defined as follows:

$$\Delta = \begin{bmatrix} \frac{\partial}{\partial x} & 0 & 0 \\ 0 & \frac{\partial}{\partial y} & 0 \\ 0 & 0 & \frac{\partial}{\partial z} \\ \frac{\partial}{\partial y} & \frac{\partial}{\partial x} & 0 \\ 0 & \frac{\partial}{\partial z} & \frac{\partial}{\partial y} \\ \frac{\partial}{\partial z} & 0 & \frac{\partial}{\partial x} \end{bmatrix} \tag{3.2}$$

- *Kinematic compatibility* between displacements and strains

$$\varepsilon = \Delta u \tag{3.3}$$

  where ε and u are the strain and displacement vectors respectively

- *The constitutive (material) law* between stresses and strains

$$\sigma = C(\varepsilon - \varepsilon_0) \tag{3.4}$$

  where C is elasticity (constitutive) matrix and ε_0 is initial strain vector.

The equations (3.1)-(3.4) along with boundary conditions formulate *strong form* of the boundary value problem. In order to solve it, a point-wise equilibrium needs to be obtained, which means that a solution is found exactly at every material point. However, usually it is difficult to solve these equations analytically for many reasons e.g. complicated geometry, boundary conditions, complex loading function,etc. Therefore, the FEM can be introduced as a numerical approach by which the differential equations (3.1)-(3.4) can be solved approximately. That means that *strong form* can be reformulated into equivalent *weak form* of a boundary value problem where equilibrium is fulfilled not for every material point but in a weighted average sense.(Bell [6])

Approximate nature of the FEM is based on the assumption of a displacement field within a certain element. Typically, a shape functions are used to describe a displacement pattern within an element by means of displacement interpolation between nodal degrees of freedom. Hence, in order to minimize an error of approximation and obtain a reasonable solution, one must be aware of how different elements behave under various conditions. (Moan [10])

Nonlinear Finite Element Method

For solving linear structural mechanical problems finite element analysis is established on the assumptions of small displacement and material elasticity.(Moan [10]) However, linear FEM theory cannot be applied for solving structural stability problem of flexible risers in catenary

configuration because nodal displacements are not small and do not depend linearly on applied forces, while strains remain small. In addition, varying contact conditions between the structure and seabed or between inner layers of the riser are known to be a significant source of nonlinearity.

The major nonlinear FEM effects are as follows (Moan [10]) :

- Non-linear geometry
- Non-linear material properties
- Non-linear boundary conditions
- Non-linear hydrodynamic loading

When it comes to solving nonlinear FEM problems, iterative and incremental methods are widely used. It is convenient to express equilibrium condition in a differential form (Moan [10]):

$$dR = \frac{d(K(r)r)dr}{dr} = K_I dr \tag{3.5}$$

where dR ,dr are load and displacemnt increments accordingly and the incremental (tangent) stiffness K_I can be expressed as:

$$K_I = \frac{d(K(r)r)}{dr} = K_0 + K_G \tag{3.6}$$

where K_0 and K_G are linear (initial) and geometric stiffnesses respectively and can be seen in the Figure 3.1.

Very often in scientific articles devoted to structural instability problems the value of tangent stiffness is monitored in order to verify the condition when buckling occurs. This is quite convenient way of doing it because of the fact that when a load reaches buckling capacity, the value of the tangent stiffness drops down to 0, which corresponds to the scenario depicted on the right side of the Figure 3.1.

Nonlinear structural problems can be solved in many different ways applying various solution techniques. However, one of the most frequently used solution procedures is a load incrimination with Newton-Raphson iteration method. The general algorithm can be represented in

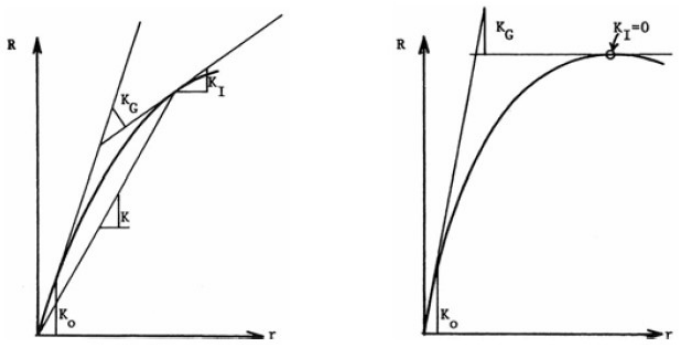

Figure 3.1: Stiffness concept at stable point (left side) and at unstable point (right side) (Moan [10])

the following way (Moan [10]):

$$r_{n+1} - r_n = \delta r_{n+1} = K_I^{-1}(r_n)(R_{ext} - R_{int}(r)) \tag{3.7}$$

where n is the iteration number; δr is the change in the displacement vector; R_{ext}, R_{int} are external and internal loads. Iteration procedure should be stopped when required accuracy is fulfilled. Displacement difference between two iterations can be set as accuracy criterion and vector norm can be applied.(Sævik [16])

3.2 The non-linear FEM software Bflex2010

For the present thesis the main tool for building a non-linear FEM models and torsion buckling analysis performance is the Bflex2010. It is FEM based computer program that was originally developed by SINTEF Civil and Environmental Engineering as part of the project Service Life Analysis of Deepwater Risers. It has a broad user group with such company representatives as Statoil, Norsk Hydro, Seaflex, Aker, etc. (Sævik [16]) The program allows a user to perform a broad scope of work related to non-linear finite element analysis of a slender marine structures. Unique advantage of the Bflex2010 is in possibility of performance of detailed local analysis taking into account complex multilayered cross-sections.

The structure of the Bflex2010 is based on several following modules. The information is extracted from (Sævik [16]) and provided in the Table 3.1.

Module	Function
BFLEX2010	• Reading and controlling of all input data • Structural analysis performance
BFLEX2010POST	• Results' post processing • Generation of ASCII files from the result database
PFLEX	• Pressure spiral bending stress analysis
BOUNDARY	• Transverse cross-sectional stress analysis
LIFETIME	• Fatigue calculation
XPOST 3D	• Result visualization, graphical user interface

Table 3.1: Bflex2010 modules and their functions

Motion kinematics in BFLEX2010

In Bflex2010 motion kinematics are based on **the Corotated Total Lagrangian formulation (CTL)**, which means that each element has local coordinate system, from which element's deformations and forces are referred. Important to maintain transformation between local element and global systems. This is done by means of transformation matrix which is continuously updated for all elements. The example of 3D beam element with CTL formulation can be seen in the Figure 3.2. Applying CTL formulation, the Green strain tensor along with 2nd Piola Kirchoff stress have to be used. (Sævik [19])

Rotational motions and deformations are determined by orthonormal base vector triad i_i^n at each node. Referring to the Figure 3.2 the rotational deformations can be obtained as relative difference between orthonormal base vector triads i_i^a, i_i^b and element reference system j_i. Other local deformation is found also by performing transformation of the i_i^n system into the j_i. (Sævik [19]), (Sævik [16])

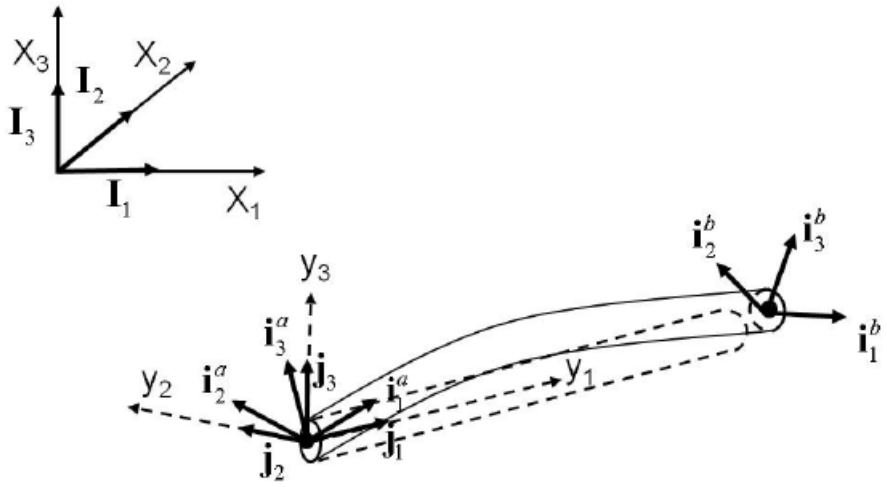

Figure 3.2: 3D beam with CTL formulation (Sævik [19])

3.3 Analytical stability problem of beams under compression and torsion

The spatial buckling problem of beams subjected to torsion and axial forces has been studied since the 19 century. The first derivation of instability expression under these conditions was done by A.G. Greenhill in the work called "On the Strength of Shafting When Exposed Both to Torsion and End Thrust" in 1883. The formula received the name of her author and can be derived in the following way according to procedure described in (Bazant and Cedolin [5]).

Let's consider a geometrically perfect beam, which is exposed to torsion moment Mt and compressive axial force P. The beam with length l and bending stiffness EI has following boundary conditions: both ends are restrained in y and z directions. It can be seen in the Figure 3.3.

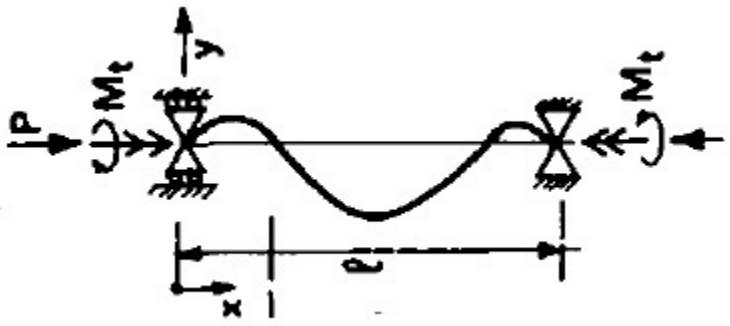

Figure 3.3: Beam under torsion moment and axial force (Bazant and Cedolin [5])

The differential equilibrium equations for the beam subjected to compressive axial force P without torsion moment can be written as follows:

$$EI\frac{d^2w(x)}{x^2} = -Pw(x) \tag{3.8}$$

$$EI\frac{d^2v(x)}{x^2} = -Pv(x) \tag{3.9}$$

where $w(x)$ and $v(x)$ are displacements in z and y directions. The torsion moment vector **Mt** consists of bending component $M_{tz} = M_t\frac{dv}{dx}$ in z direction and component $M_{ty} = -M_t\frac{dw}{dx}$ in y direction. Combining the torsion components with Eq.(3.8),(3.9), the following differential equations are obtained:

$$EI\frac{d^2w(x)}{x^2} - M_t\frac{dv}{dx} + Pw(x) = 0 \tag{3.10}$$

$$EI\frac{d^2v(x)}{x^2} + M_t\frac{dw}{dx} + Pv(x) = 0 \tag{3.11}$$

The general solution can be expressed in the following form

$$v = Ae^{i\omega x} \qquad\qquad w = Be^{i\omega x} \tag{3.12}$$

Substituting Eq.(3.12) in Eq.(3.10),(3.11), the following system of homogeneous linear equations are acquired:

$$\begin{bmatrix} P - EI\omega^2 & iM_t\omega \\ -iM_t\omega & P - EI\omega^2 \end{bmatrix} + \begin{bmatrix} A \\ B \end{bmatrix} = 0 \tag{3.13}$$

To find the solution, determinant of the first matrix should be 0, which gives Eq.(3.14)

$$EI\omega^2 \pm M_t\omega - P = 0 \tag{3.14}$$

Taking into account only positive torque $+M_t$, the roots of Eq.(3.14) can be found

$$\omega_{1,2} = \frac{1}{2EI}(-M_t \pm \sqrt{M_t^2 + 4EIP}) \tag{3.15}$$

Coming back to the general solution, which is the real or imaginary part of

$$v = A_1 e^{i\omega_1 x} + A_2 e^{i\omega_2 x} \qquad w = B_1 e^{i\omega_1 x} + B_2 e^{i\omega_2 x} \tag{3.16}$$

where A_1, A_2, B_1, B_2 are constants, which can be complex. Applying the boundary conditions $v = w = 0$ for both ends of the beam $x = 0 \, and \, x = l$, the equation systems (3.17) are determined.

$$\begin{cases} A_1 + A_2 = 0 \\ A_1 e^{i\omega_1 l} + A_2 e^{i\omega_2 l} = 0 \end{cases} \qquad \begin{cases} B_1 + B_2 = 0 \\ B_1 e^{i\omega_1 l} + B_2 e^{i\omega_2 l} = 0 \end{cases} \tag{3.17}$$

In order to find non-zero solution for equations (3.17) , the condition of $e^{i\omega_1 l} = e^{i\omega_2 l}$ should be maintained, which means that $\omega_2 l = \omega_1 l + 2\pi n$,where n is integer. This can be written in a following way for n=1:

$$\omega_2 = \omega_1 + 2\pi / l \tag{3.18}$$

Combination of Eq.(3.18) and Eq.(3.15) gives Eq.(3.19)

$$\frac{\pi}{l} = \frac{\sqrt{M_t^2 + 4EIP}}{2EI} \tag{3.19}$$

After some simple mathematical transformation Eq.(3.20) can be rearranged as:

$$\frac{M_t^2}{(\frac{4E^2 I^2 \pi^2}{l^2})} + \frac{P}{(\frac{EI\pi^2}{l^2})} = 1 \tag{3.20}$$

where $\frac{4E^2 I^2 \pi^2}{l^2} = (M_{cr}^0)^2$, $M_{cr}^0 = \frac{EI\pi k}{l}$ $k = 2$, M_{cr}^0 -the critical torsion moment for buckling without axial force and $\frac{EI\pi^2}{l^2} = P_{cr}^0$, P_{cr}^0 - the critical compressive axial force for buckling without the torsion moment.

Eq.(3.20) is the Greenhill's formula and it can be represented in a more convenient way:

$$(\frac{M_t}{M_{cr}^0})^2 + \frac{P}{P_{cr}^0} = 1 \tag{3.21}$$

The graphical interpretation of the Greenhill's formula Eq.(3.21) is illustrated in the Figure 3.4.

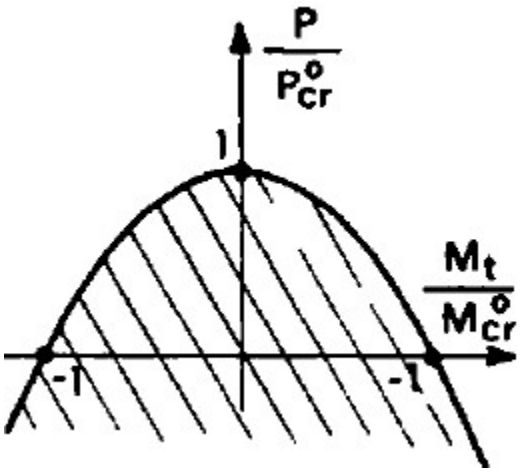

Figure 3.4: Graphical interpretation of the Greenhill's formula (Bazant and Cedolin [5])

In the technical report (Liu [8]) the author shows that in case of applied tensile load $T = -P$ the Eq.(3.20) can be rewritten as:

$$\frac{M_t^2}{(\frac{4E^2I^2\pi^2}{l^2})} = \frac{T}{(\frac{EI\pi^2}{l^2})} + 1 \tag{3.22}$$

Considering the large value of the beam length l, the term $\frac{T}{(\frac{EI\pi^2}{l^2})} \gg 1$. Hence, $\frac{M_t^2}{(\frac{4E^2I^2\pi^2}{l^2})} = \frac{T}{(\frac{EI\pi^2}{l^2})}$. (Liu [8])

As consequence of that, the torsion moment can be computed as follows:

$$M_t = \sqrt{4TEI} \tag{3.23}$$

Chapter 4

BFLEX2010 straight beam model

4.1 Introduction

Prior to the analysis of the torsion buckling of flexible risers in the catenary shape, the simplified elastic straight beam model is built in the BFLEX2010 with the purpose to test it and find out how well the results of critical torsion load computed by the program correspond to the analytical solution based on the Greenhill's formula Eq.(3.21).

The model represents a pretensioned straight beam with bending stiffness $EI = 5.03\,kNm^2$. At the one beam's end which is fixed in all directions except of X-axis, the tension force T of 0.984 kN is applied.[1] While at the other beam's end which is clamped, the prescribed rotation θ_x around X-axis is imposed and monitored until the torsion instability occurs. The sketch of the model is provided in the Figure 4.1.

Figure 4.1: Straight beam model

Analytically the moment can be calculated from Eq.(3.22). However, the result depends on

[1] Note that the values for EI and T will be used also later on for catenary configuration.

beam length l. Substituting the values of EI, T and different l in the Greenhill's Eq.(3.21), the Figure 4.2 is obtained. Hence, it can be seen clearly from the graph that the critical torsion

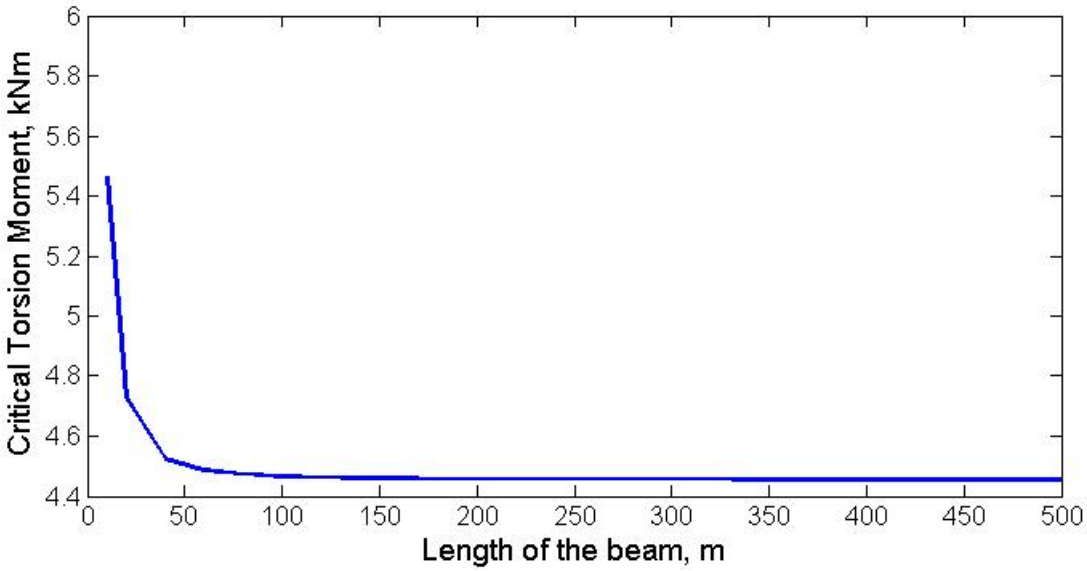

Figure 4.2: Analytical solution for different beam lengths l

reaction remains unaffected for large values of the beam length l. Based on this fact , the l for the modeling is selected to be equal 100m which corresponds to the critical torsion moment Mt of 4.47 kNm.

4.2 Modeling

Applied elements and material characteristics

The model of 100m beam is built up in BFLEX2010 using **PIPE31** element type, which is 3D 2-noded Euler-Bernoulli beam element with linearly elastic behavior. Selected material properties are shown in the Table 4.1.

Axial stiffness (EA)	409.0 MN
Bending stiffness about Y-axis (EI_y)	5.03 kNm^2
Bending stiffness about Z-axis (EI_y)	5.03 kNm^2
Torsion stiffness (GI)	1.0 MNm^2

Table 4.1: Elastic material properties

Applied boundary conditions

In the BFLEX2010 three types of boundary conditions (BC) may be assigned: local, global, special. To apply BC, node ID number and nodal degrees of freedom (DOF) should be specified. In case of 3D model each node has 6 DOFs, where DOF1, DOF2, DOF3 are related to translations in X, Y, Z directions respectively and DOF4, DOF5, DOF6 are linked to rotations about X, Y, Z axes.

In case of the simplified beam model, the global BC is used exactly as it depicted in the Figure 4.1 i.e. at the beam's clamped end DOFs1-6 are restrained, and at the free-to-move beam's end DOFs2-4, DOF6 are suppressed.

Applied loads

The axial tensile force, gravity load and prescribed rotation θ_x about X-axis are exerted to the beam in the way it is shown in the Figure 4.1. The main idea is that prescribed rotation θ_x is imposed at the clamped end (which overwrites the DOF4 BC) until the torsion buckling happens.[2] At the same time, the reaction torsion moment M_x is monitored along the deformational process with the purpose to select the largest value - critical torsion moment M_x^{crit}.

The BFLEX2010 straight beam model is presented in the Figure 4.3.

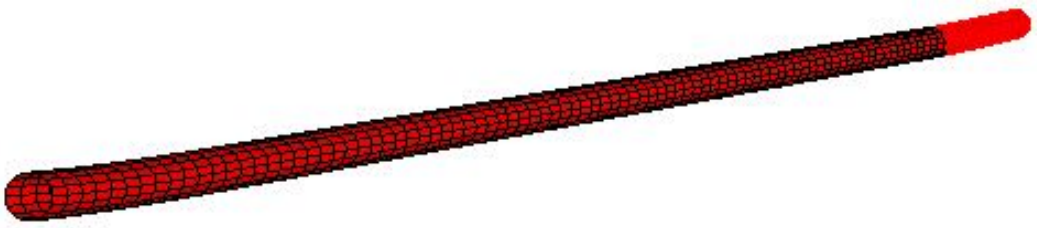

Figure 4.3: BFLEX2010 Straight beam model

4.3 Buckling analysis of the model

Mesh size sensitivity

In order to get stable solution, the sensitivity analysis using different mesh sizes is performed starting from very coarse mesh and ending up with the refined one. The simulations were car-

[2] It is worthwhile to implement rotation very slowly and smoothly for the sake of numerical convergence.

ried out for the following mesh sizes : 1m , 0.5m , 0.2m , 0.1m. For each case the critical torsion moment M_x^{crit} (torsion buckling moment) is identified and plotted along the whole beam length. The results are reflected in the Figure 4.4, and the main outcome is that *the mesh size of 20cm or less gives stabilized solution.*[3]

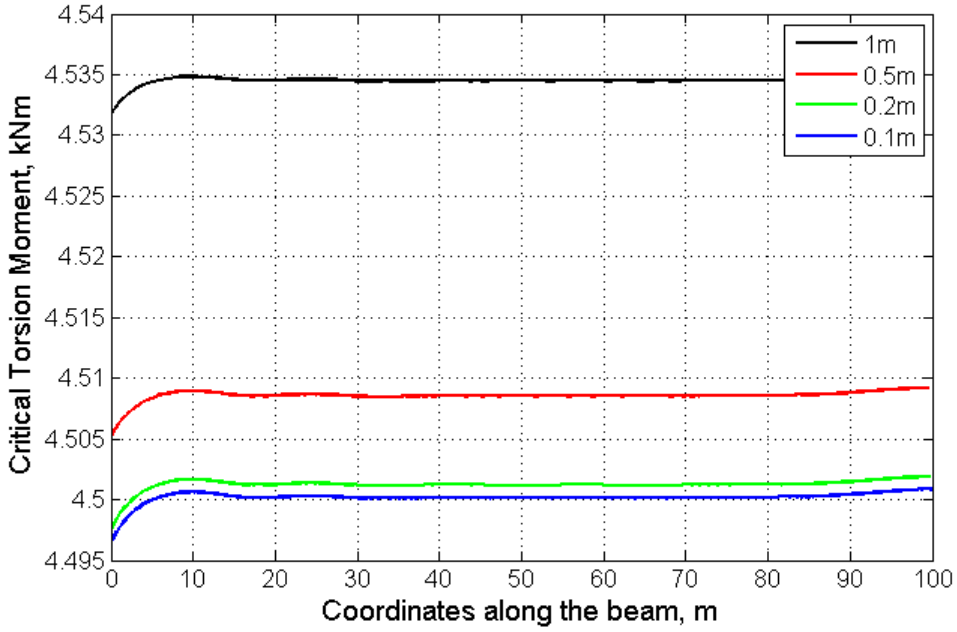

Figure 4.4: Analysis of mesh size sensitivity

Buckling performance of the model

In order to examine the global torsion buckling phenomenon closely, the reliable model with well convergent mesh of 0.1 m is selected. The Figure 4.5 reveals the result of reaction torsion moment M_x against imposed axial rotation θ_x computed by the BFLEX2010. The critical value of the moment M_x^{crit} when the global buckling occurs is 4.5 kN. Comparing this value to the critical moment of 4.47 kN calculated previously by the Greenhill's formula, one can conclude the deference between them is considerably small (0.85% with respect to analytical solution). *Hence, using the BFLEX2010 for solving the stability problem of beams under axial and torsion forces enables a user to obtain reliable results in compliance with the theoretical solution.*

[3]This is important conclusion because the mesh size of the models in the next chapters will be based on this fact.

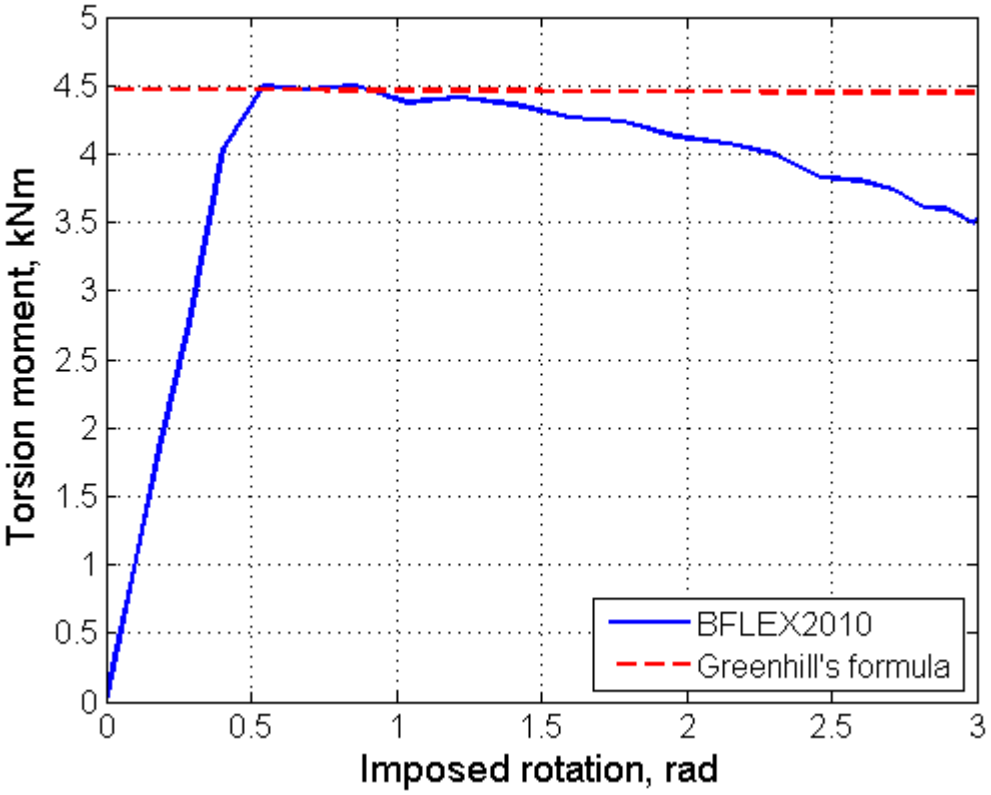

Figure 4.5: Torsion buckling of the straight beam model with 10 cm mesh size

Chapter 5

BFLEX2010 elastic catenary model

5.1 Introduction

The Figure 5.1 shows typical riser catenary configuration. During the operation of installation, the riser's top angle is very large , almost vertical. Tension along the riser's length decreases from the sea surface down to the bottom, the place called the Touch Down Zone (TDZ). When it

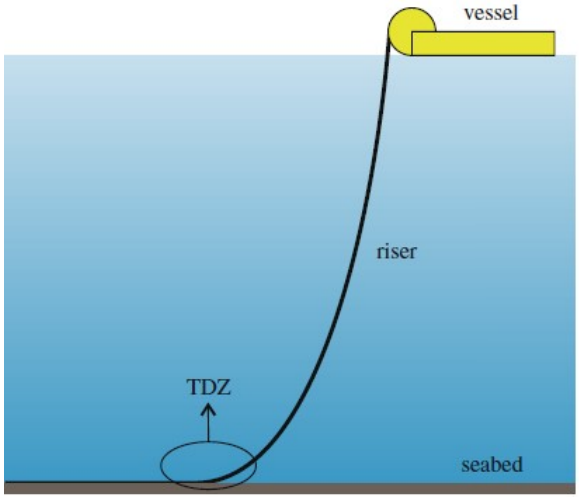

Figure 5.1: Catenary riser (Neto and Martins [11])

comes to the structural stability of the flexible risers in the catenary configuration subjected to the torsion and tensile loads, TDZ represents the area of primary concern due to a very low tension level. Therefore, applying torsion load, buckling process can happen in that region transferring torsion energy into bending energy. Consequently, a loop can be formed and turned into

a kink causing a severe damage.

The ultimate goal of this chapter is to thoroughly describe the physics of that intricate process using the BFLEX2010 program and verify how reasonable it is to apply the Greenhill's analytical expression for catenary shaped beam to predict torsion buckling. In order to fulfill that, the non-linear FEM model is built in the BFLEX2010 based on the catenary riser model from the article by (Neto and Martins [11]).

Hence, the riser with the top angle α of 89.6 deg, the external diameter d_e of 0.12m and the submerged weight w_s of 140.3 N/m is taken into account for the constant depth scenario with d=1000m. However, the values of the catenary length S and the horizontal bottom tension T_0, which are illustrated in the Figure 5.2, are not provided in (Neto and Martins [11]).

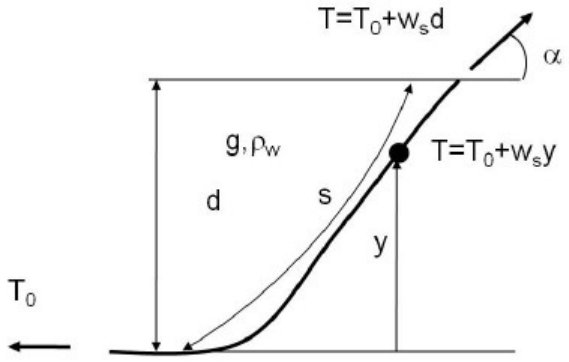

Figure 5.2: Global catenary geometry (Sævik [19])

Without them it is impossible to build the model. Therefore, they can be calculated using following equations taken from (Sævik [19]) :

$$S = \sqrt{d^2 + 2d\frac{T_0}{w_s}} \tag{5.1}$$

$$tan\alpha = \frac{w_s S}{T_0} \tag{5.2}$$

$$\frac{tan\alpha^2 T_0^2}{w_s^2} - 2d\frac{T_0}{w_s} - d^2 = 0 \tag{5.3}$$

Substituting the values of α, w_s and d into Eq.(5.3) and solving quadratic equation, the TDP tension is found to be T_0=986.4 N. After that, in order to find S, T_0 should be used in Eq.(5.1). Hence, S is computed to be 1007 m.

5.2 Case studies

Three case studies taken from (Neto and Martins [11]) are used in order to evaluate the torsion buckling capacity of the riser and the role of the seabed friction:

- *Case study A* stands for the riser model which does not include the region of the riser laid on the seabed. In other words, it is 1007 m line connecting the TDP and the point on the free surface. Hence, the TDP in that condition remains in the same place.
- *Case study B*. The model includes the riser piece of 1007 m from the case study A plus the flowline section of 600m resting on the seabed without friction. In contrast to the case A, the position of the TDP for this case can vary.
- *Case study C*. The model is the same as for the case B except for the one thing. The riser's tale of 600 m has the Coulomb friction coefficients in axial direction μ_x of 0.4 and in lateral direction μ_y of 1.0.

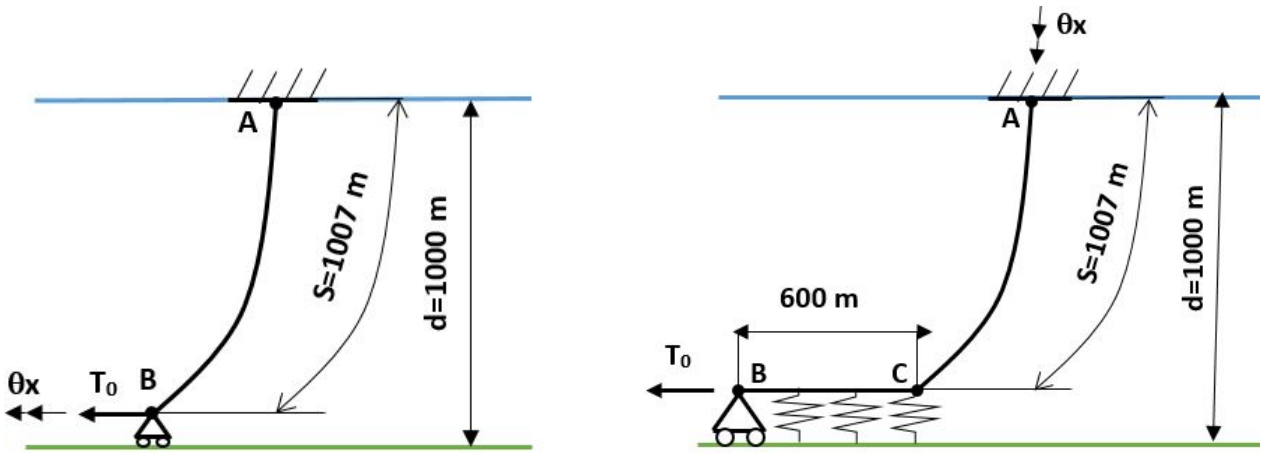

(a) $CaseA$ (b) $CasesB, C$

Figure 5.3: Study cases

The sketches of the study cases are depicted in the Figure 5.3. In order to investigate critical buckling torsion moment, the same strategy applied as in the Chapter 4 for the straight beam model. Therefore, prescribed axial rotation θ_x is exerted in the TDP or in the riser's end at the free surface depending on the study case, and torsion moment is monitored as constrained reaction. From the Figure 5.3a it can be seen that for the model A, θ_x is imposed in the point B, while

the point A of the riser is totally fixed. The Figure 5.3b demonstrates that for the study cases B and C , θ_x is applied at the free surface in the point A , while the point B remains rotationally fixed.

5.3 Modeling

5.3.1 Applied elements and material characteristics

The same set of the BFLEX2010 elements was used to assemble the models for discussed above study cases. Applied elements are represented in the Figure 5.4.

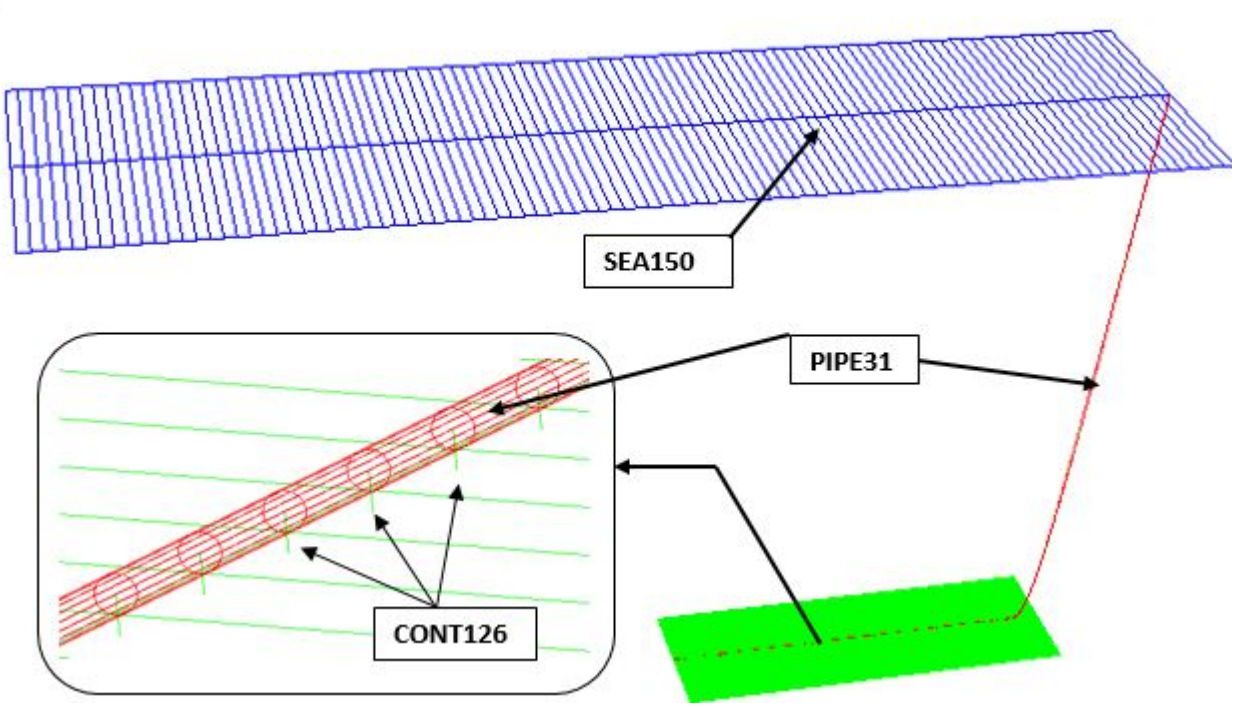

Figure 5.4: Applied BFLEX2010 elements for elastic catenary model

PIPE31 element type (see section 4.2) was chosen to model purely elastic riser behavior. The material properties of the **PIPE31** correspond to the one utilized for the straight beam model and can be observed in the Table 4.1.

The riser has the long length, but the buckling deformation process occurs only in the region close to the TDP. Hence, relying on the mesh sensitivity analysis in the Section 4.2, the refined mesh size of 0.1 m is applied to the riser's section in the vicinity of the TDP, while for the rest of

the riser the coarse mesh size of 1 m is considered.

The free surface of the sea is created by the **SEA150** 4-noded element. The density of the water is assigned to be 1024 $\frac{kg}{m^3}$.

In order to maintain the seabed-riser interaction, the contact elements **CONT126** are implemented. **CONT126** elements connect the contact surface describing the flat seabed and the **PIPE31** elements. Time for activation of the contact elements can be specified by a user. When it is done, spring is established at the pipe node.

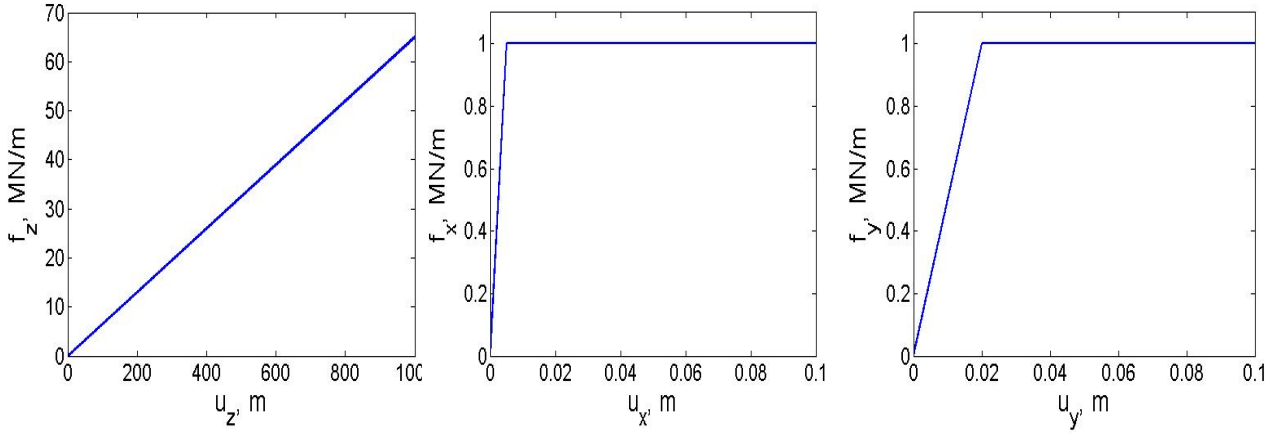

(a) Vertical resistance (b) Axial resistance (c) Lateral resistance

Figure 5.5: Material models of the soil resistance in three directions

There are two options in BFLEX2010 for setting the material model of soil resistance: **HYCURVE** model and **EPCURVE** model. **HYCURVE** gives hyper-elastic (non-linear elastic) material behavior, while **EPCURVE** stands for elastoplastic material characteristics with kinematic/isotropic hardening. (Sævik et al. [20]) For modeling vertical riser-soil interaction **HYCURVE** model is taken into account. It is illustrated in the Figure 5.5a . Where, f_z is a vertical soil reaction force per meter and u_z is a vertical displacement. However, **EPCURVE** model was carried out for the soil resistance (Coulomb friction force) in axial and lateral directions. It is reflected in the Figures 5.5b, 5.5c .Where, f_x and f_y mean unit resistance in axial and lateral directions, and u_x, u_y are axial and lateral displacements respectively. The Coulomb friction coefficients μ_x, μ_y corresponding to f_x, f_y can be set by a user. For the frictionless case study B: $\mu_x = 0, \mu_y = 0$, while for the case study C: $\mu_x = 0.4, \mu_y = 1$.

5.3.2 Applied loads and boundary conditions

In order to investigate the torsion buckling of the riser, the catenary configuration should be obtained. The models for all study cases are built in the way that in the beginning of analysis straight beam representing the riser rests on the seabed. Then, prescribed vertical displacement applied in the one end of the beam to lift it up to the sea surface. This is done by running static analysis in the BFLEX2010. During vertical displacement imposition the beam axially slides on the seabed. Therefore, the contact elements **CONT126** are not activated during this process with the purpose of avoiding friction force.

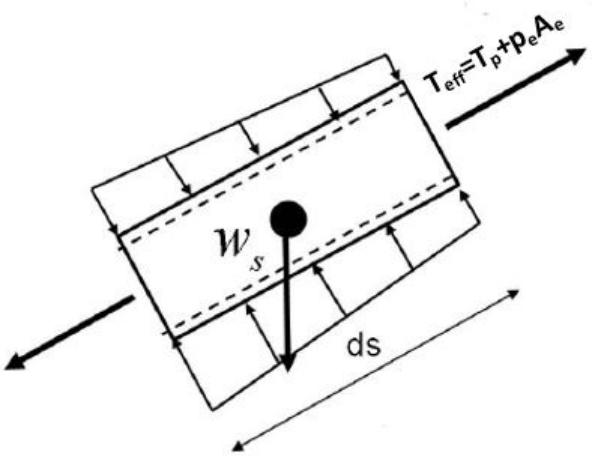

Figure 5.6: Submerged weight and effective tension of the riser's segment. (Sævik [19])

Once the catenary configuration is established, a watertight riser's segment into the water is subjected to the loads, which are shown in the Figure 5.6. Where, w_s is submerged weight (dry weight + buoyancy force), T_{eff} is effective tension consisting of pipe wall tension T_p and component from external pressure p_eA_e. (Sævik [19])

Considering the Figure 5.3 , the TDP tensile load T_0 calculated in the Section 5.1 is applied for all study cases. In BFLEX2010 this is done by using concentrated nodal load in the riser's end B (see Figure 5.3).

Having the submerged weight and the TDP tension load utilized for the catenary shaped riser, prescribed axial rotation is ready to be induced. The contact elements are activated in order to take into account friction effects. Procedure of axial rotation imposition needs to be performed in sufficiently slow way in order to avoid numerical errors related to inertial effects. From the Figure 5.3a it can be seen, that for the case study A axial rotation is applied in the riser's

end B (all DOF are restrained except DOF1, DOF5), while the end A is kept totally restrained. For the case studies B and C axial rotation is implemented in the riser's end A, while all DOFs for the end B are restrained except DOF1 and DOF5 (see Figure 5.3b). Along the deformation process the torsion reaction moment is monitored.

5.4 Buckling performance of the models

Obtained results

For three case studies two types of analysis were carried out in BFLEX2010. Static analysis was performed to achieve the riser catenary configuration. However, the torsion stability study was done by using dynamic analysis.

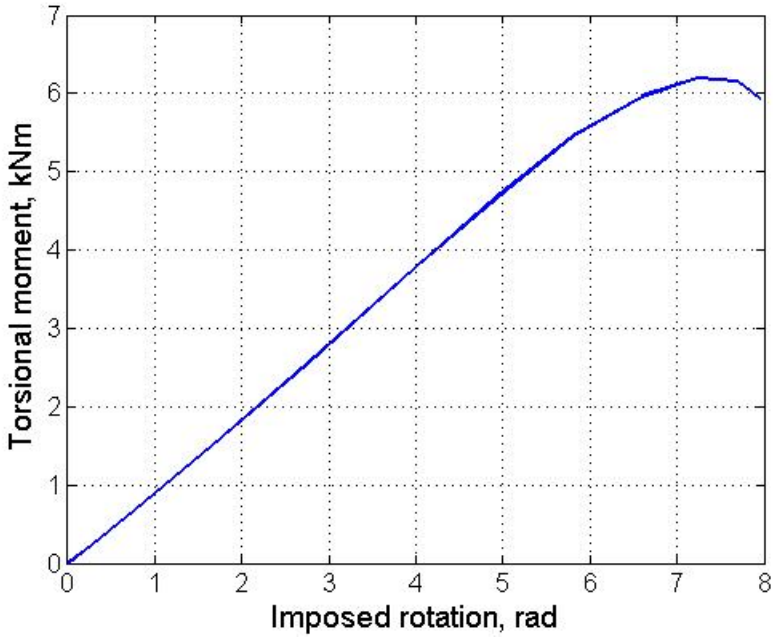

Figure 5.7: Torsion behavior for the case study A

The Figure 5.7 demonstrates the result of the case study A. Initially, the torsion reaction moment follows linear behavior (until the prescribed rotation value of roughly 6rad). The structure experience some deformations in the TDP region due to very low tension. After linear section, softening curve pattern of the torsion moment takes place until the global collapse of the structure. When the torsion moment reaches its peak, the torsion buckling occurs and the riser forms

kink. This deformational pattern represents severe failure. It is shown in the Figure 5.8.

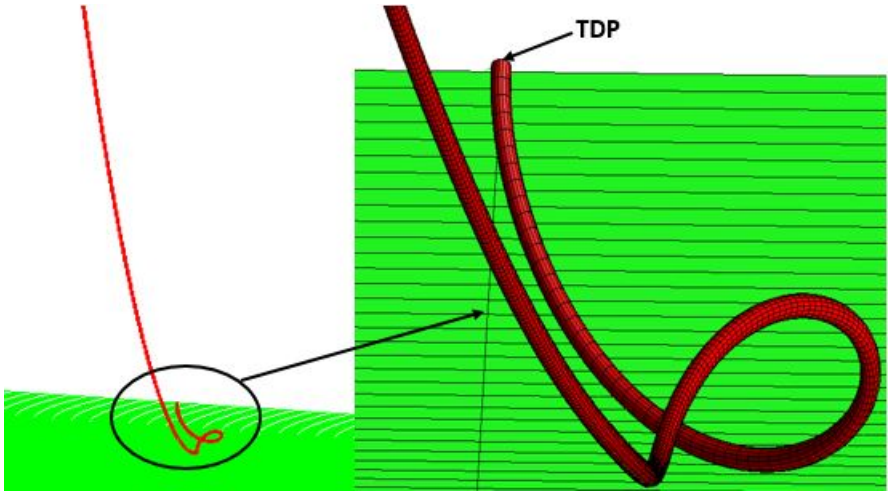

Figure 5.8: Deformation pattern for the case study A

For the case studies B and C the plots of torsion moment against prescribed rotation follow similar trend as for the case study A (see Figure 5.9).

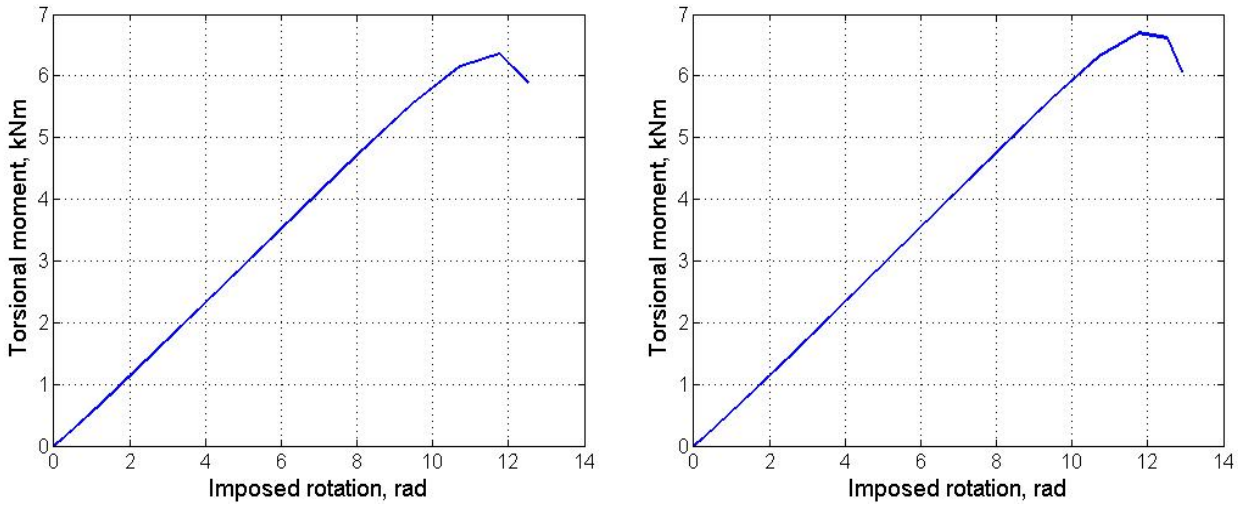

(a) Case B (b) Case C

Figure 5.9: Torsion behavior for the case studies B and C

However, the deformational behavior of both cases are different from the case A because the position of the TDP varies during the rotation imposition. From the Figure 5.10 it can be noticed that for the frictionless case B, the TDP is significantly shifted in transverse direction from the center line of the riser's seabed section. This does not happen for the case study C , where the

frictional forces restrain the TDP movement. This is well illustrated in the Figure 5.10 for the moment when the buckling occurs.

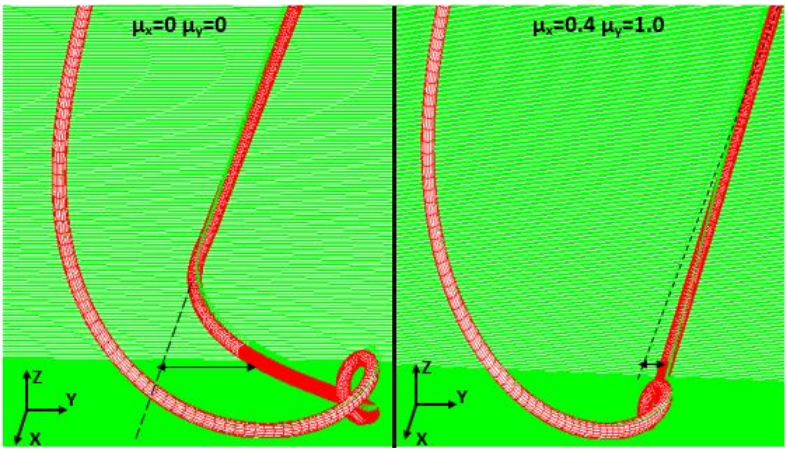

Figure 5.10: Deformation patterns for the case study B (left) and the case study C (right)

The physics of the loop formation process

During the process of axial rotation imposition, out-of-plane deformations of the riser start in the TDP region due to very low tension compare to the tension in the riser's section hanging in the water. Thus, the torsion energy transfers into the bending energy. The length of the riser's section subjected to bending deformations (triggered by torsion) is decided to be called "**activated length**". **Activated length** characterizes the region where kink is likely to be formed. The limits of **activated length** can be determined by plotting out the development in time of the reaction moments around Z axis and Y axis M_z, M_y along the whole length of the structure.

To demonstrate the way how **activated length** can be identified, the case study C as the most realistic one (due to the friction effects) is chosen to be an example. For that case the prescribed axial rotation is applied during 20 second. The rotation is linearly distributed starting with $\theta_x = 0\,rad$ at $t = 0\,s$ and $\theta_x = 14\,rad$ at $t = 20\,s$. The Figure 5.11 shows how the reaction bending moments M_y, M_z are developed over the time. The horizontal axes of the Figures 5.11a,5.11b stands for the coordinate along the riser starting from 0 m at the sea surface riser's end A (see Figure 5.3b). Looking at these graphs, **the activated length** of the riser can be found as the section where M_z and M_y deviate from zero. For the case C with the TDP coordinate of 1007m, **the activated length** is located within the interval with following coordinates [990m,1015m]. (See

Figure 5.11). The yellow line curves of the Figures 5.11a,5.11b corresponding to t=16s represent M_y, M_z along the riser's length when the buckling occurs. At t=17.5s M_y, M_z (black color curves) are substantially larger than for the time moment when buckling happens , which means that the structure experience large deformations increasing the size of the formed kink.

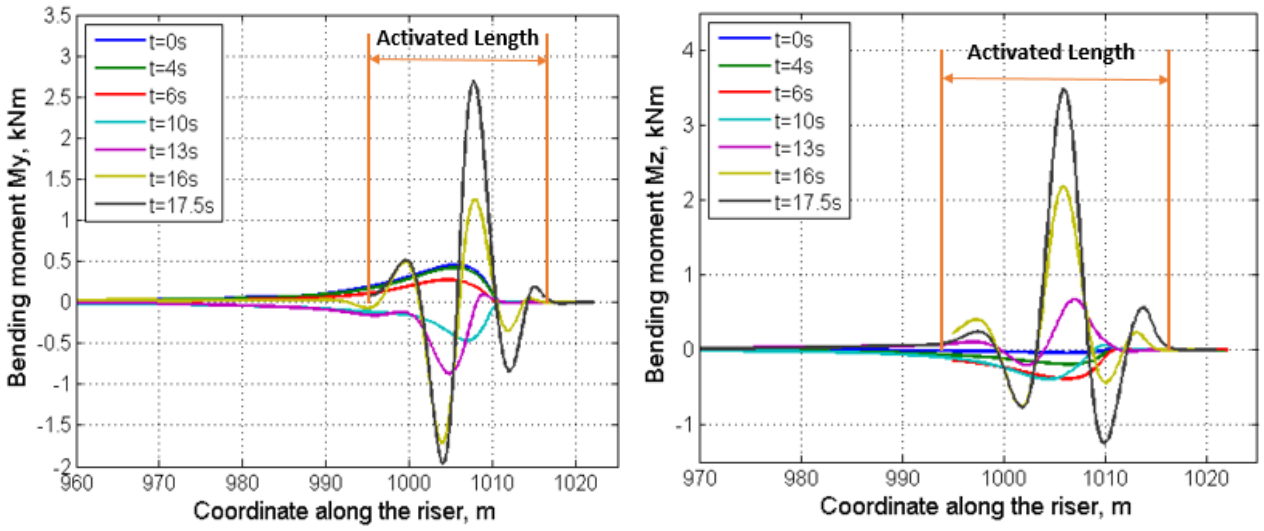

(a) My (b) Mz

Figure 5.11: Bending behavior for the case study C in the activated region

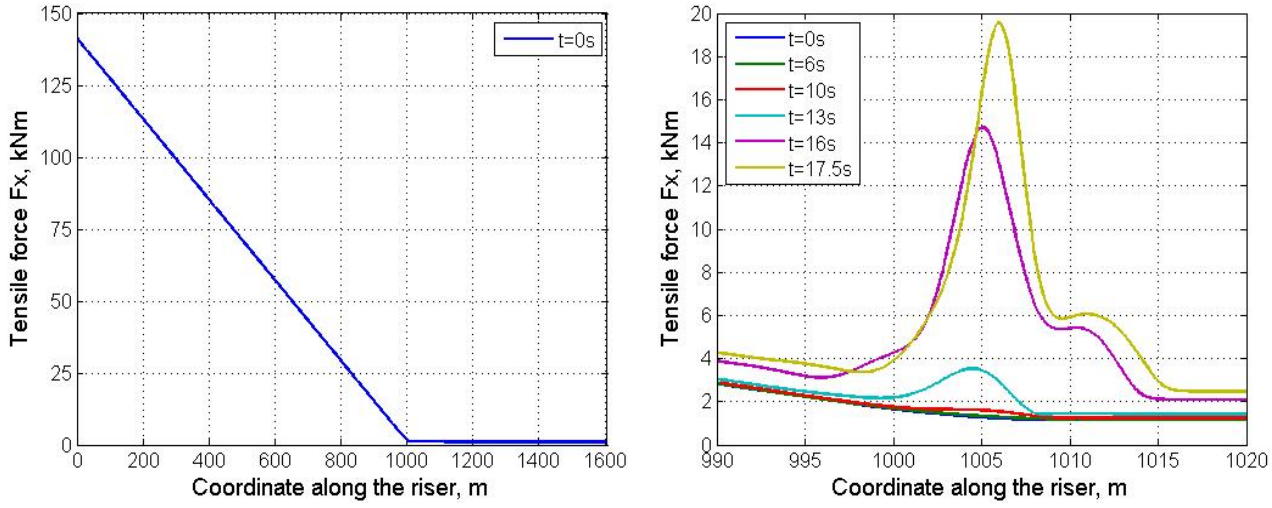

(a) Along the whole riser's length at t=0s (b) Along the activated section

Figure 5.12: Tensile reaction force for the case study C

Another important finding is that kink formation process triggers increase in tension reaction force along the activated length. The Figure 5.12b shows how the tension is developed with

time. At the time when the torsion buckling occurs (16 s), the maximum tensile force in the activated region is 7 times higher than for undeformed catenary configuration (t=0 s).

5.5 Discussion of the results

Comparing the case study B and the case study C, the latter is more realistic (due to soil friction forces). However, from engineering standpoint, the former one is a better choice for prediction of the critical torsion moment because it gives smaller critical moment value. Physically, this is due to the fact, that frictionless case B has larger **activated section** hanging in the water (see Figure 5.10), which gives less tension in the TDZ than for the case C.

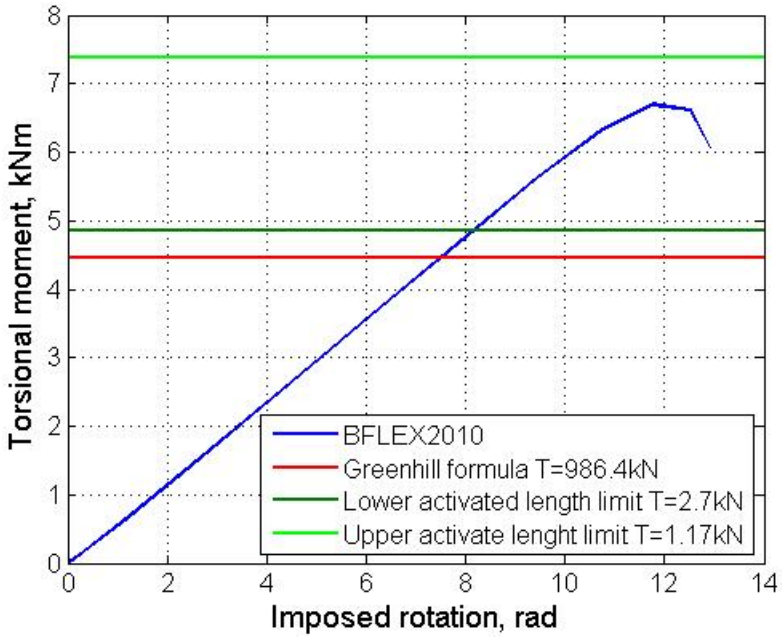

Figure 5.13: Influence of tension variation on critical torsion moment

Substituting the TDP tensile force T_0=986.4 N into the Greenhill's formula Eq.(3.21), the critical torsion moment can be found. The analytical result for all three study cases is the same due to the large length of the beam and is found to be M_t=4.46kNm. However, this theoretical result is valid for straight beam with constant tension. In the case with catenary configuration tension varies along riser's length from the sea surface down to the TDP. The example of such tensile reaction force variation is illustrated in the Figure 5.12a. Additionally , tensile force in

activated section tends to increase significantly during the process of prescribed rotation implementation. Therefore, the critical torsion moment value is expected to be larger than the one obtained by the Greenhill's equation. Substituting tension values (See Figure 5.12b for t=0s) at the beginning of **the activated length** (the upper limit corresponding to riser's coordinate of 1015 m) with T=1.17 kN and at the end of **the activated length** (the lower limit corresponding to riser's coordinate of 995 m) with T=2.7 kN in the Greenhill's expression, gives a range of the critical torsion moment where the accurate value is expected to be found. This can be observed in the Figure 5.13. The result of the critical torsion moment obtained by BFLEX2010 is within the range. Though this result deviates by 1.5 kNm from the one obtained in (Neto and Martins [11]), it is believed to be correct based on the excellent agreement between the BFLEX2010 and the analytical solution demonstrated in the previous Chapter 4 for the simplified beam model.

Chapter 6

COMPIPE42 model

6.1 Introduction

Previously, in the Chapters 5,4 the models are characterized by linearly elastic material behavior. In that cases bending moment-curvature relation looks like it is shown in the Figure 6.1a, where EI_e stands for linearly elastic bending stiffness. However, it is more realistic to use non-linear

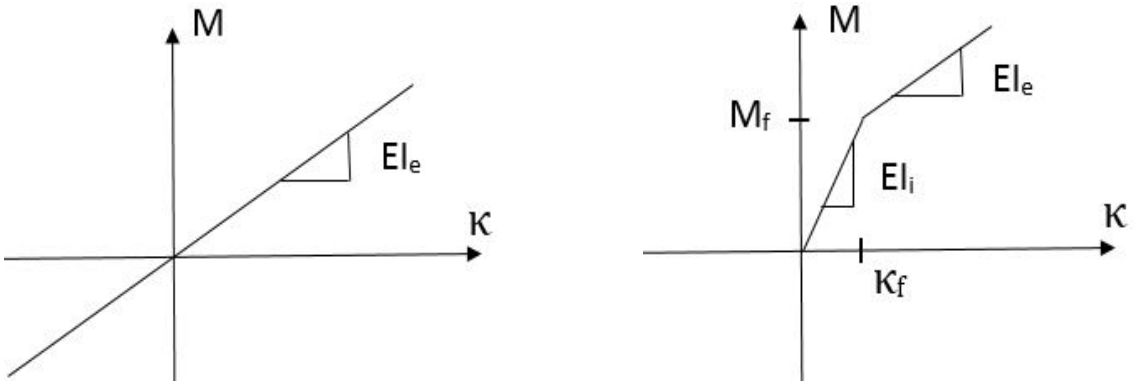

(a) Linear case (b) Non-linear case

Figure 6.1: Moment-curvature relations

material model in order to describe flexural response of the riser. As can be seen from the Figure 6.1b, the riser has very high stiffness (EI_i- initial stiffness) for small values of curvature, κ. This is because of the friction forces, which prevent relative slip between tensile armored layers.(Sævik [17]) However, when bending moment M overcome the value of friction moment (M_f), tensile layers start to slide relative to each other and the stiffness of the riser reduces significantly to the

value of EI_e.[1] (Sævik [17])

Bending properties of the riser is very important for torsion stability in catenary configuration due to the transformation of the torsion energy bending energy causing flexural deformation process. Therefore, the main purpose of this chapter is to analyze how complex non-linear material behavior in bending can influence torsion buckling phenomenon for riser in catenary configuration.

6.2 Influence of friction moment M_f on torsion buckling

6.2.1 Parametric study

To investigate the impact of non-linear moment-curvature behavior on torsion buckling of the riser in catenary configuration, the COMPIPE42 model is created in BFLEX2010. This model is based on the case study C from Chapter 5 (as the most realistic case). COMPIPE42 model is built up in the same way as linearly elastic model of the case C except for one difference, that **COMPIPE42** beam elements are used instead of **PIPE31** elements.

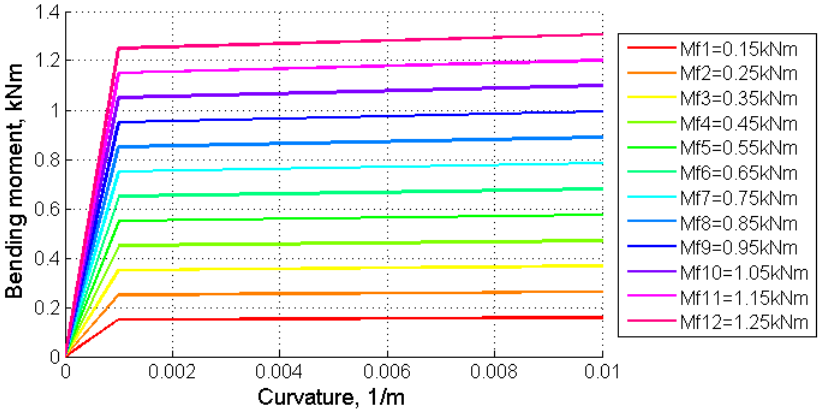

Figure 6.2: **EPCURVE** material models for parametric study

Non-linear material bending properties for **COMPIPE42** elements are specified by using **EPCURVE** material model consisting of two regions. First one is determined by initial stiffness due to friction moment and the second region is defined by elastic stiffness of 5.03 kNm^2 from the case C.

[1] For more details about riser's behavior in bending see Section 1.4.

For parametric study of torsion buckling under various friction moments, range of the friction moment M_f is selected between 0.15 and 1.25 kNm. The non-linear material **EPCURVE** models are created corresponding to according M_f. They are represented in the Figure 6.2.

The boundary conditions and the process of the loads imposition are exactly the same as for the case study C. To avoid numerical mistakes, the loads have to be applied sufficiently slow.

6.2.2 Results discussion

Numerous simulations are carried out in the BFLEX2010 for different friction moments with a purpose to determine torsion buckling . Due to non-linear material characteristics the reaction torsion moment does not remain constant along the length of the riser during rotation imposition as it does for the linearly elastic model. Therefore, it is not possible to determine visually the exact moment when buckling occurs (for each time step the reaction moment has different variation along the riser's length).

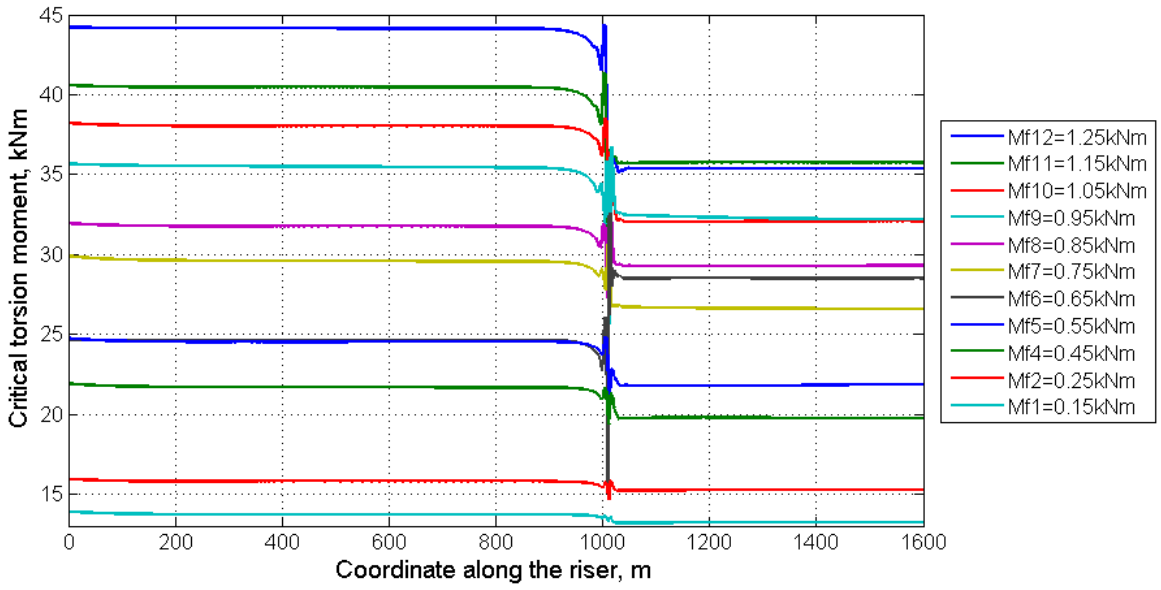

Figure 6.3: Critical torsion moment variations along the riser length for COMPIPE42 model

The main question then is how to determine the critical torsion moment. To answer that the average value of the torsion moment distribution along the riser's length needs to be computed for every time step of the deformation process. After that, the maximum value should be selected. This value is a reasonable choice for the critical torsion moment.

Figure 6.3 shows the results of torsion moment distributions along the riser's length, which give the critical moment values. Analyzing the Figure 6.3, one can find out that the larger friction moment is, the larger variation in torsion moment is going to be. For example, for the smallest friction moment value the moment distribution looks like a straight line, while for the friction moment of 1.25 kNm the moment variation can be of the order of 10 kNm. *Hence, important conclusion can be drawn that the increase in material nonlinearities gives rise in deviation of the reaction torsion moment along the riser's length.*

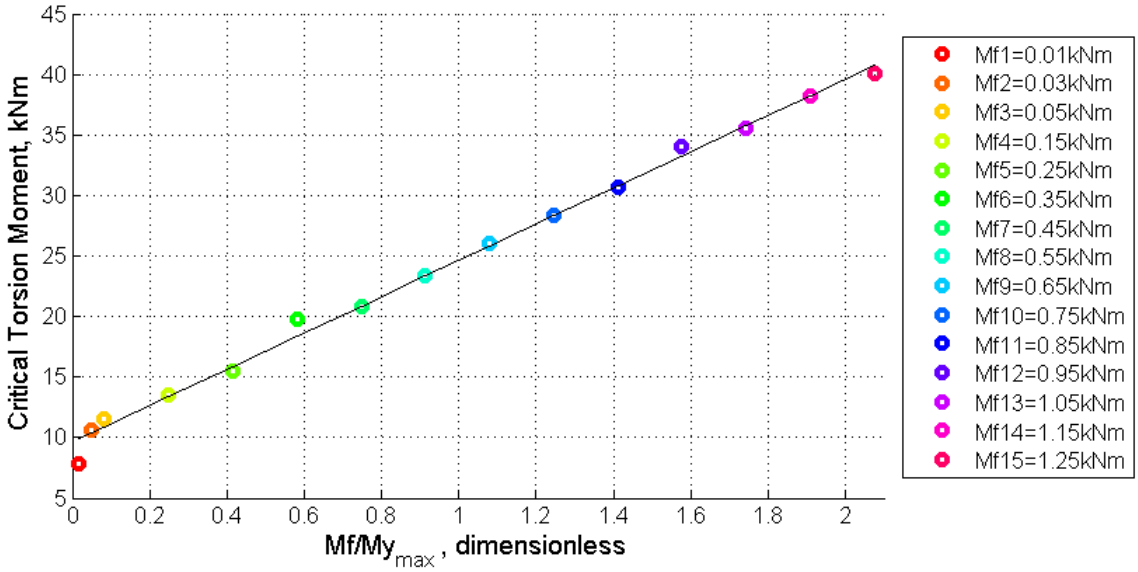

Figure 6.4: Torsion buckling results for COMPIPE42 model

Additionally to previous results, some more simulations are performed for different values of M_f. The critical torsion moments are computed for each value of M_f and plotted out in the Figure 6.4 against the fraction $\frac{M_f}{My_{max}}$, where My_{max} is the maximum bending moment along the whole length of the riser around y-axis (at the moment when catenary configuration is built up and prescribed torsion rotation is no applied yet) for linearly elastic study case C. From the Figure 6.5 My distribution along the riser's length can be seen and the maximum value of it My_{max}=0.602 kNm.

The main outcome of the parametric study is that non-linear material behavior of the riser significantly affects torsion buckling capacity. The bigger friction moment M_f is utilized , the larger critical torsion moment is going to be obtained. From the Figure 6.4 one can see, that for

the very low value of the M_f the critical torsion moment approaches to the value computed for linearly elastic case C (when M_f=0).

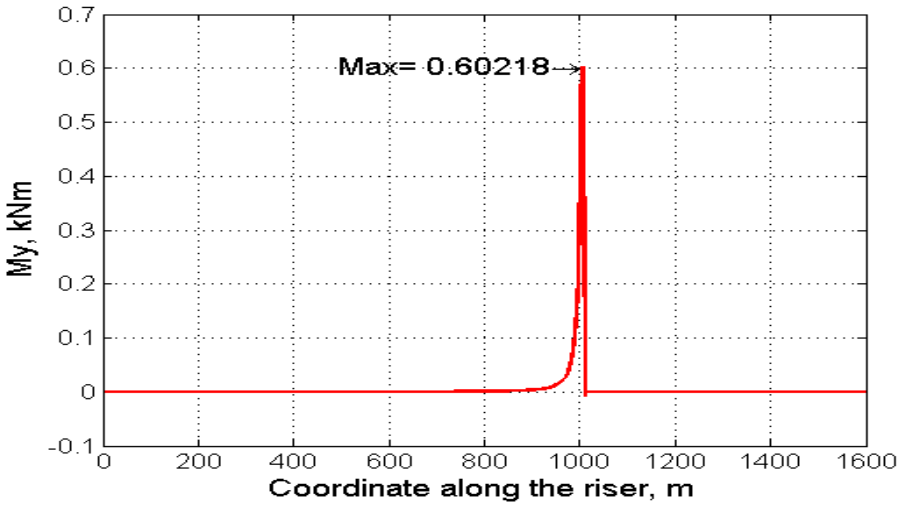

Figure 6.5: Bending moment My for the case study C

The example of deformational behavior for COMPIPE42 model with M_f=0.65 kNm when torsion buckling occurs is provided in the Figure 6.6. Torsion buckling triggers severe failure with the kink formation process.

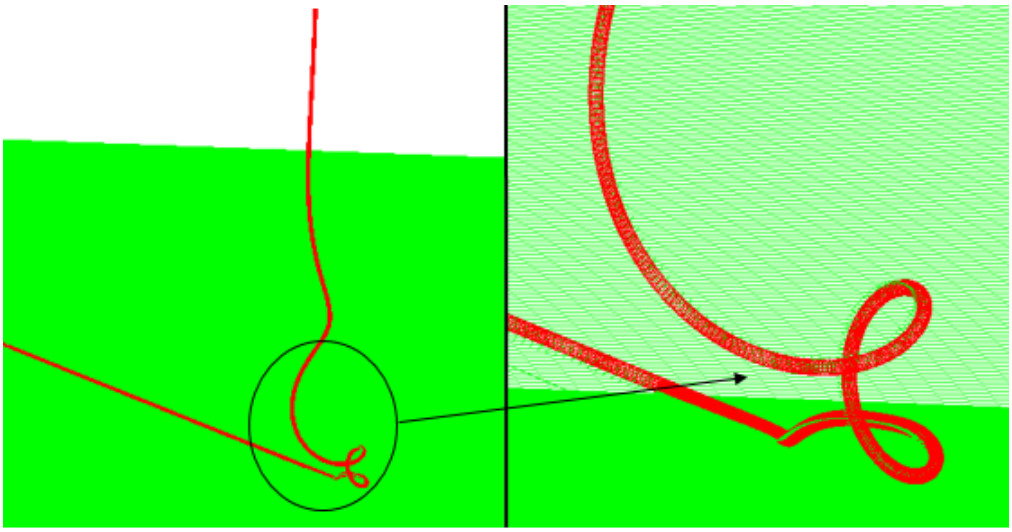

Figure 6.6: Deformation pattern for COMPIPE42 model with M_f=0.65 kNm

6.3 Influence of tension/torsion coupling β parameter on torsion buckling

6.3.1 Introduction

COMPIPE42 elements enable a user not only to create a models with non-linear material behavior but to take into account the physics of axial strain in tensile armor of a flexible pipe. This can be done by activation of β parameter influencing the interaction between tensile and torsion strain components.

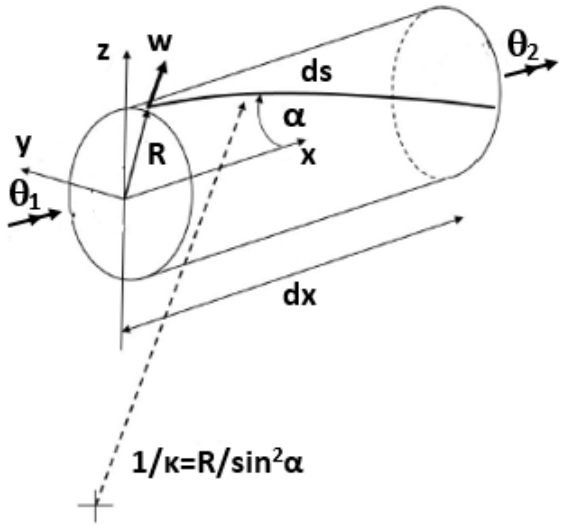

Figure 6.7: Axisymmetric deformation parameters (Sævik [19])

All forces (tension,external pressure,torsion) that were applied for all models in this thesis belong to axisymmetric type. The response of the riser due to such loads is governed by characteristics of the tensile armor layers. Mathematically this can be described in the following way. With reference to the Figure 6.7, axial strain in tensile armor ε_s can be determined by centerline strain ε_x, torsion $\tau = \frac{\theta_2 - \theta_1}{dx}$, lay angle $\tilde{\alpha}$ and radial displacement of the helix w.(Sævik [19])

$$\varepsilon_s = \varepsilon_x cos^2(\tilde{\alpha}) + Rcos(\tilde{\alpha})sin(\tilde{\alpha})\tau + \frac{w}{R}sin^2(\tilde{\alpha}) \tag{6.1}$$

Introducing tension/torsion coupling β parameter as $\beta = Rcos(\tilde{\alpha})sin(\tilde{\alpha})$ and neglecting ra-

dial displacement of the helix w, Eq.(6.1) can be rewritten as follows:

$$\varepsilon_s = \varepsilon_x cos^2(\tilde{\alpha}) + \beta\tau \tag{6.2}$$

Then, applying the energy principles for Eq.(6.2), the axial stiffness of **COMPIPE42** element can be determined and it is clear that it will be affected by tension/torsion coupling β parameter.

6.3.2 Parametric study

Parametric study regarding the influence of β parameter on torsion buckling of the riser in catenary configuration is carried out. Multiple simulations with different values of β parameter were

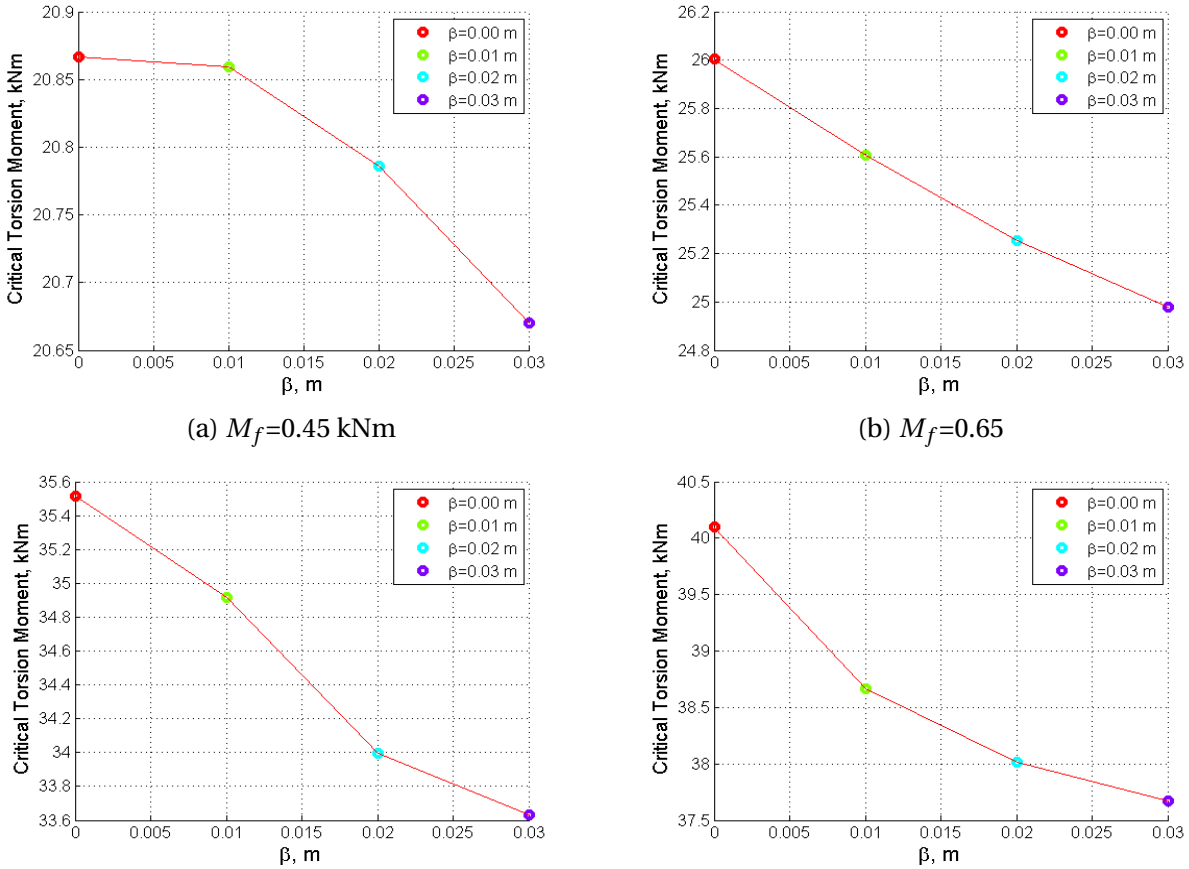

(a) M_f=0.45 kNm (b) M_f=0.65

(c) M_f=1.05 (d) M_f=1.25

Figure 6.8: β parametric study

performed for COMPIPE42 models at different levels of M_f taken from previous Section 6.2. Some results are represented in the Figure 6.8. There is no need to provide the results for every

case of M_f because the outcomes follow similar trends and well described in the conclusions below.

Main conclusions from this parametric study are as follows:

1. *The influence of tension/torsion coupling β parameter on critical torsion moment is not significant (see Figure 6.8). For the COMPIPE42 models with small M_f approaching the value of 0.01 kNm this influence is negligible.*

2. *Larger value of β gives smaller value of critical torsion moment.*

3. *The impact of β parameter on critical torsion moment is more influential for the COMPIPE42 models with large M_f. For instance, results of the critical torsion moment from the Figure 6.8a is much more affected by β than results from the Figure 6.8d.*

Chapter 7

Dynamic criterion for evaluation of kink formation

7.1 Introduction

For such offshore operation as riser installation cyclic heave motion of the vessel is a very important factor because it influences tensile force variation in the TDZ. Changes in the TDP tension can significantly reduce torsion buckling capacity of the riser. Therefore, the main purposes of this chapter are to describe the physical process of how heave dynamics of the system can influence kink formation of the riser and to establish criterion for safe operation limiting heave motion of the vessel.

Very often the vessel changes its direction (laying route) introducing axial rotation to the system. Having that in combination with heave cyclic load can be extremely dangerous and cause severe torsion failure of the riser ending up in a kink formation.

Having initial torsion utilized in the system, torsion energy is transfered into bending energy. If, in addition to that, the riser tarts to rock in heave, this will inevitably bring more energy and substantial contribution to the bending. Adequate measure of how much the structure is bent can be total riser curvature κ_t about centroid along the whole riser's length. In order to obtain it, both contributions: y-curvature κ_y and z-curvature κ_z should be considered and the following formula Eq.(7.1) needs to be used.

$$\kappa_t = \sqrt{\kappa_y^2 + \kappa_z^2} \tag{7.1}$$

7.2 Role of the curvature

To demonstrate an example of how total curvature along the riser length can be found, the linearly elastic model from the case study C (see Chapter 5) is selected. Applying prescribed torsion rotation at upper end of the riser, there will be moment in time when the torsion buckling occurs. When this happens, the section of the riser located in close proximity of the TDP (so called activated length region, see Section 5.4) is dramatically deformed. This can be seen from the

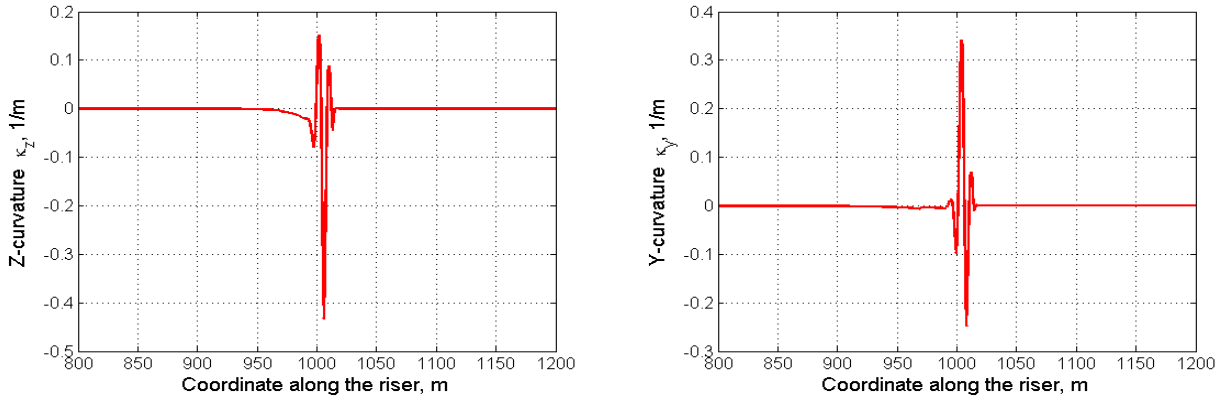

(a) κ_z (b) κ_y

(c) κ_t

Figure 7.1: Curvature along the riser's length when buckling happens, elastic Case study C model

Figures 7.1a, 7.1b clearly representing deformed section of the riser within activated length and also undeformed riser section, where κ_y and κ_z remain of 0 1/m. Applying Eq.(7.1), the Figure 7.1c is built up and the maximum value of κ_t is identified.

As it was shown in the Section 5.4, from the beginning of prescribed torsion rotation imposition till the moment when torsion buckling takes place, there will be development of bending

process with subsequent loop formation. This can be tracked by monitoring reaction bending moments M_y and M_z (what exactly is done in the Section 5.4, see Figure 5.11). Curvatures κ_y and κ_z are well correlated with M_y and M_z respectively. Therefore, another way of measuring the extent of flexural riser deformations in the activated zone due to torsion load is to monitor development of maximum total curvature value during utilization of torsion reaction moment M_x. Figure 7.2 illustrates the growth of the curvature along the deformation process in case of

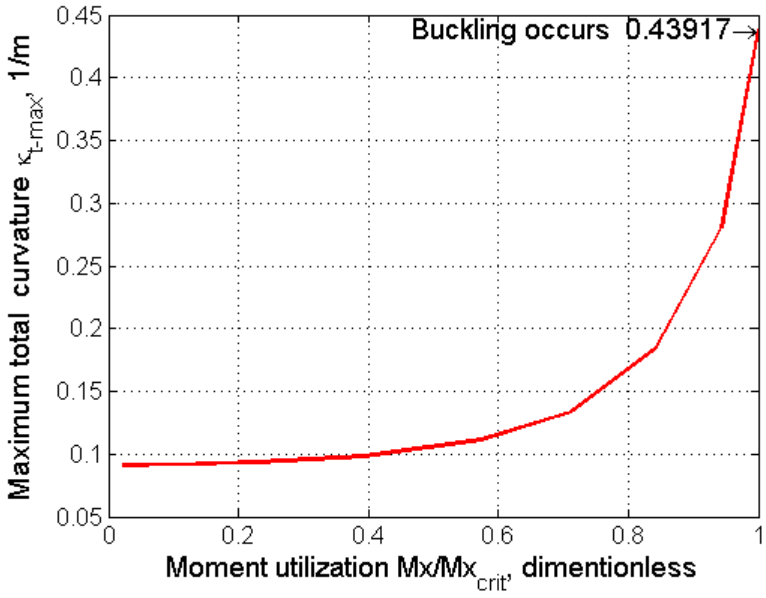

Figure 7.2: Development of the maximum value of the total curvature for elastic model

elastic model from the Case study C.

Critical value (when buckling occurs) of the maximum total curvature κ_{crit} can be a good indicator for prediction of kink formation process. For instance, if the Case study C model exceeds the κ_{crit} value of 0.439 $\frac{1}{m}$, kink will be formed in the TDZ.

7.3 Dynamic analysis of cyclic heave motion for elastic model

Elastic model from the Case study C (see Figure 5.3b) as the most realistic one is selected to perform dynamic analysis. Initially the riser rests on the sea bottom. Then during 5 second period one of the riser's end is lifted up to the sea surface in order build up catenary configuration. Following this, the prescribed torsion rotation is applied to the riser's end on the free surface (the other riser's end remains rotationally fixed) during 20 sec until 80% of the critical torsion moment is utilized. Then, the cyclic heave motion is induced in the top riser's end by introduction of prescribed vertical displacement having the following form expressed by Eq.(7.2).

$$a = a_0 sin(\frac{2\pi}{T_h}(t - t^*)) \tag{7.2}$$

Where, a_0 is heave amplitude, T_h is heave period, t^* is 25s-duration of two previous load histories and t- is time from 25 sec until 55sec. The values for a_0 and T_h are chosen to be 2m and 10sec accordingly. The load histories are represented in the Table 7.1

Time	**Load description**
0-5 s	Lifting the riser's end to the free surface (prescribed vertical displacement)
5-25 s	Imposed axial rotation in the top riser's end (prescribed axial rotation)
25-55 s	Cyclic heave motion of the top riser's end corresponding to Eq.(7.2)

Table 7.1: Load histories for dynamic analysis of elastic model

The cyclic heave load history for the top riser's end is demonstrated in the Figure 7.3.

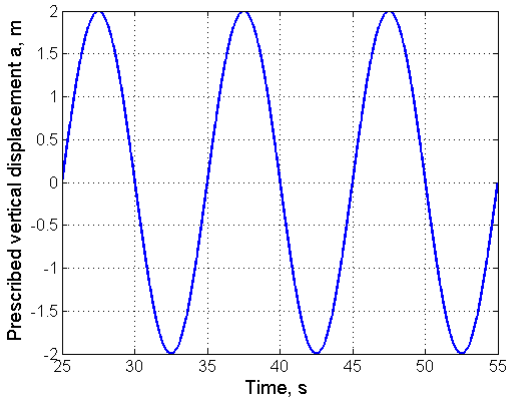

Figure 7.3: Cyclic heave load history for dynamic analysis of elastic model

In order to describe the physics of the process in the TDZ of the riser during cyclic heave load, dynamic analysis of the Case study C model under loads presented in the Table 7.1 is carried out and one element located in the activated section of the riser is selected and thoroughly investigated with respect to the reaction forces (the chosen element is highlighted in the Figure 7.5). It is done and presented in the report for one element because the other elements results in the activated region follow the same physical principles.

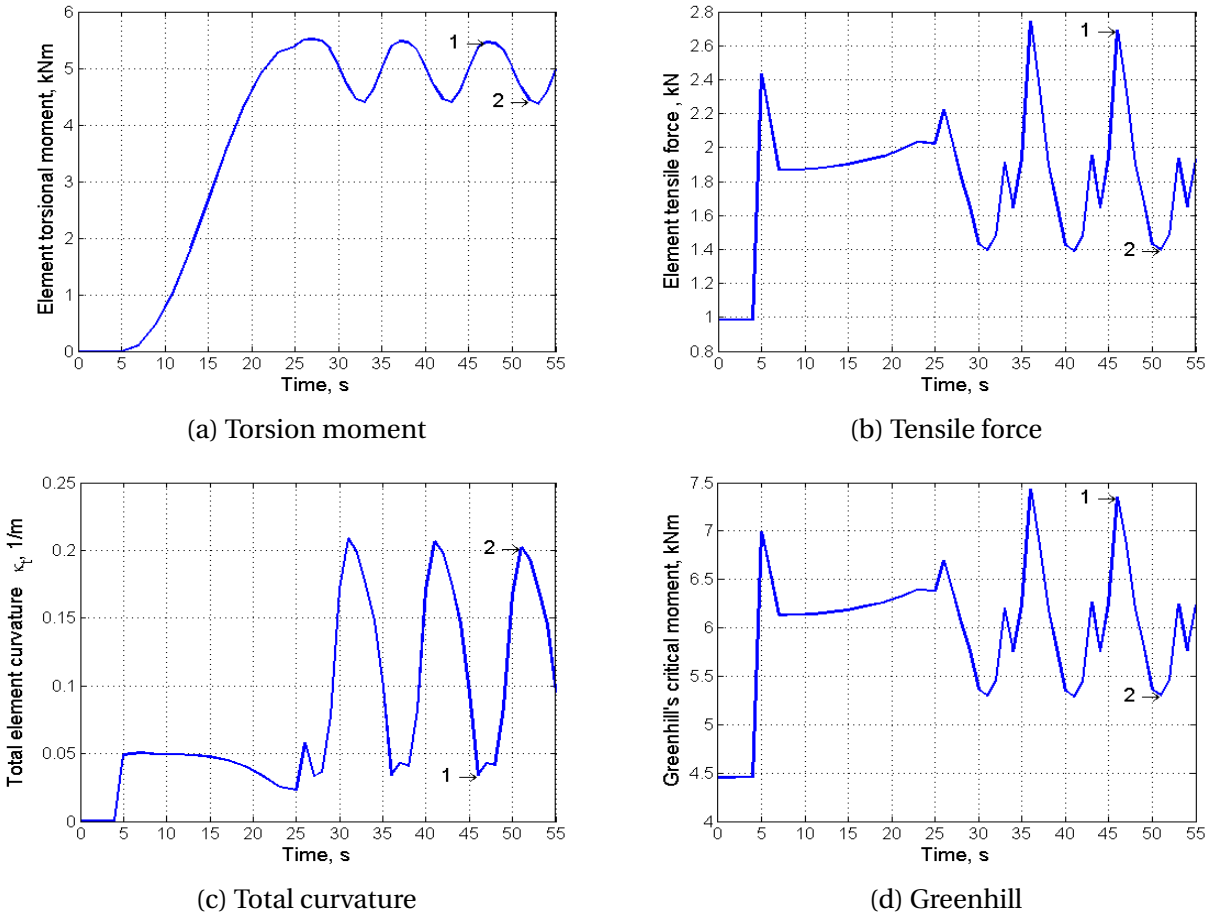

(a) Torsion moment

(b) Tensile force

(c) Total curvature

(d) Greenhill

Figure 7.4: Element results of dynamic cyclic heave analysis

Having torsion moment utilized, the heave load is imposed consisting of 3 cycles. After the first cycle from 25s to 35s, the numerical solution is stabilized which can be seen from the Figure 7.4. During each heave cycle, the system experiences the tensile force variation in the TDZ. When the riser's end is lifted above the sea level, the tension in the activated area is increased. However, when the riser's end moves below the sea surface, the tensile force will be reduced.

Looking closely at the third cycle corresponding to the time range within 45s-55s, one can

notice from the Figures 7.4a,7.4b that the element torsion moment and tensile force are well correlated between each other. The higher the riser's end is above the sea surface the higher element tensile force and corresponding reaction torsion moment will be. In the Figures 7.4a,7.4b **time point 1** shows the maximum values for tension and torsion moment when the riser's end is above the sea level and **time point 2** with the minimum values when the end is below. [1] It is very important that torsion capacity depends on tension variation. To show that, the capacity graph (see Figure 7.4d) is built up by using the Greenhill's formula Eq.(3.22).

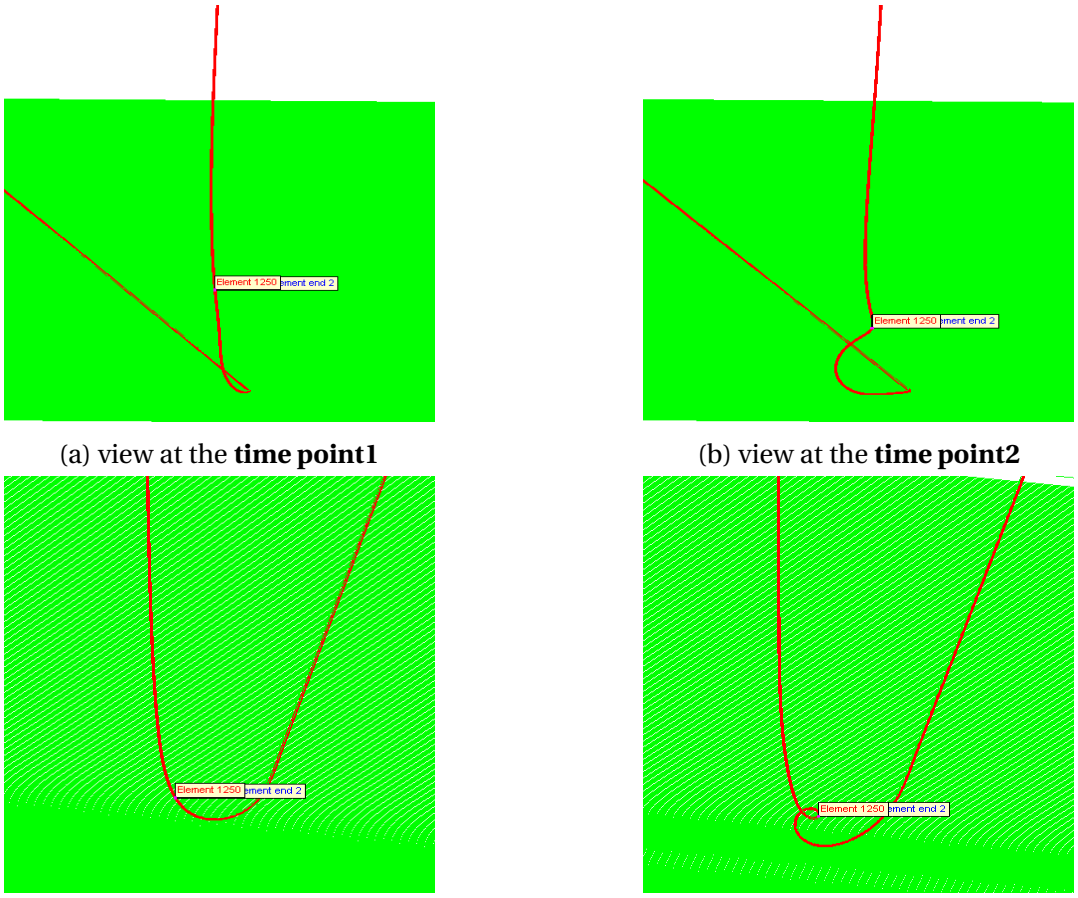

(a) view at the **time point1**

(b) view at the **time point2**

(c) another view at the **time point1**

(d) another view at the **time point2**

Figure 7.5: Visualization of deformational patterns at **time point1** and **time point2**

As all previous characteristics the element deformation also varies during the cycle, which is depicted in the Figure 7.4c. At the **time point 1** when the tensile force is maximum, the structure is stretched out and no significant deformation is observed (curvature is small). However, at the

[1] Worth to mention: not for this simulation case, but for the cases with large heave amplitude when the riser's end goes below the sea surface, tension in the activated zone can drop below zero, which means that the section of the riser in the TDZ will be compressed.

time point 2 with minimum tension there is dramatic rise in the curvature. From the Figure 7.5 revealing the deformational behaviors of the riser, it can be clearly seen that at the **time point 1** the structure in the activated zone remains undeformed, while at the **time point 2** the kink is distinctly formed.

Hence, the information about curvature variation with time for elements in the activated zone of the riser is essential for kink prediction. Tracking how the maximum value of the total curvature (among the elements in the activated zone) develops in time is the optimum procedure to evaluate kink formation. Consequently, **the dynamic criterion for evaluation of kink formation** can be formulated in the following way:
If during dynamic load cycle maximum value of the total curvature κ_{t-max} *changing with time exceeds the critical total curvature* κ_{crit} *(see Section 7.2 , e.g. for elastic case study C model* κ_{crit}*=0.439* $\frac{1}{m}$ *), kink will be inevitably formed.*

7.4 Dynamic criterion. Parametric study for elastic model

In order to show the example of how **the dynamic criterion** for evaluation of the kink formation can be applied, parametric study is carried out. Elastic Case study C model is selected and subjected to numerous dynamic analyses with the load histories described in the Table 7.1. Hence, prior to cyclic heave motion of the top riser's end, the prescribed axial rotation in the top riser's end is imposed giving the utilization of the torsion reaction moment. Therefore, the parametric analysis of cyclic heave dynamics is divided into three simulation groups:

1. Performed for the model having **25%** utilization of the critical torsion reaction moment, which corresponds to the imposed axial rotation in the top riser's end of around **3 rad**.

2. Performed for the model having **50%** utilization of the critical torsion reaction moment, which corresponds to the imposed axial rotation in the top riser's end of around **6 rad**.

3. Performed for the model having **80%** utilization of the critical torsion reaction moment, which corresponds to the imposed axial rotation in the top riser's end of around **9 rad**.

Each simulation group is exposed to cyclic heave loads with different amplitudes a_0 varying between 0.5m and 5m. The heave period T is kept to be constant of 10s. The results of the

parametric study are presented for the third circle of the heave load from 45s to 55s, where the numerical solution is stabilized. (See Figure 7.6 below). They show how the maximum value of

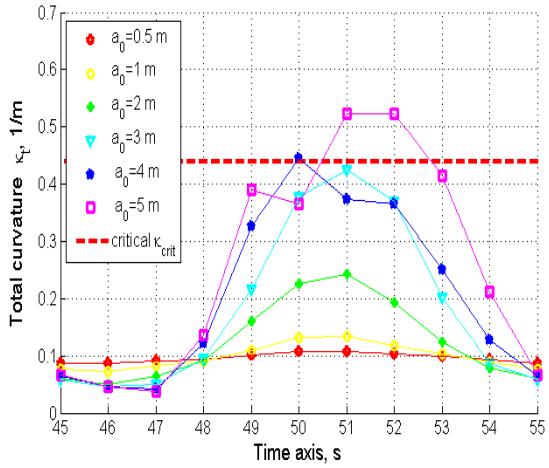

(a) Group #1 $\frac{M_x}{M_x^{crit}} = 0.25$

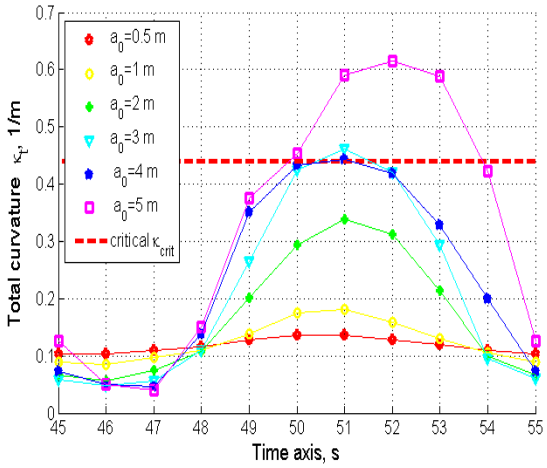

(b) Group #2 $\frac{M_x}{M_x^{crit}} = 0.5$

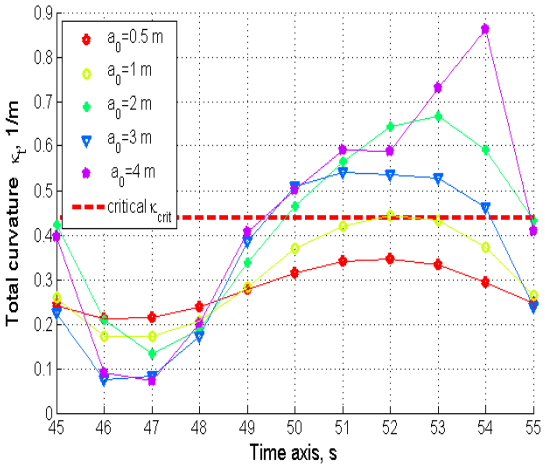

(c) Group #3 $\frac{M_x}{M_x^{crit}} = 0.8$

Figure 7.6: Development in time of the maximum value of total curvature for elastic model

the total curvature κ_{t-max} changes in time during the deformation process of the third heave cycle for each simulation case. The red dashed line stands for the critical curvature κ_{crit}. Applying **the dynamic criterion**, the time moment when kink formation occurs can be clearly identified from the graphs above. It happens when the red dashed line is exceeded by κ_{t-max} curves. If the κ_{t-max} curves lay below the red dashed line, the safe operational condition for riser installation is maintained. A discussion about introduction of safety factors reducing the value of κ_{crit} and, thus, shifting the red dashed line downwards can be also taken into account. It can substantially

mitigate risks of kink formation.

Looking at the Figure 7.6a, one can observe that for the riser with 25% utilization of the critical torsion operation with heave amplitude more than 3m can be dangerous. However, for the case with torsion reaction utilization $\frac{M_x}{M_x^{crit}}$ of 0.8 it is not acceptable even to operate with the heave amplitude of 1 m. (See Figure 7.6c).

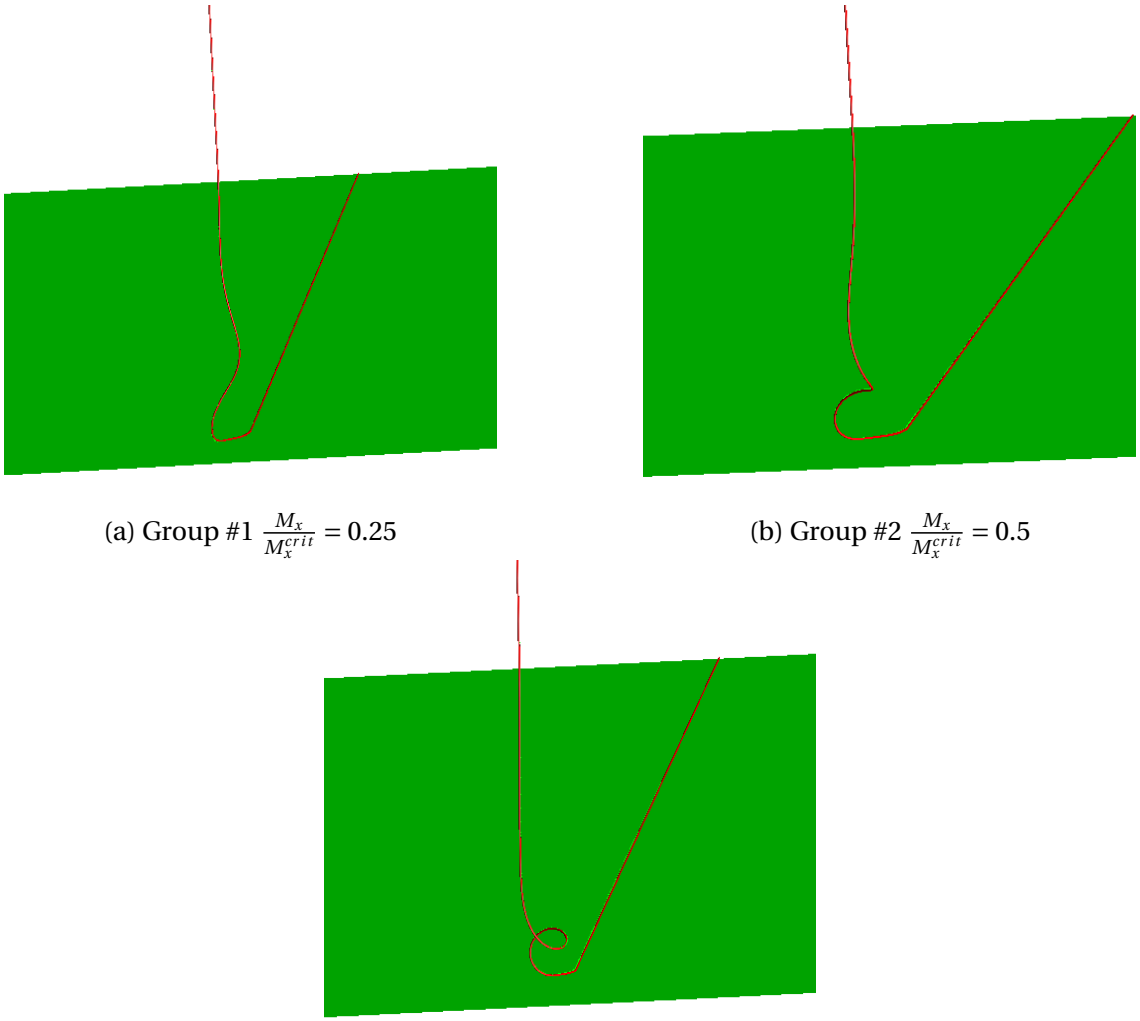

(a) Group #1 $\frac{M_x}{M_x^{crit}} = 0.25$

(b) Group #2 $\frac{M_x}{M_x^{crit}} = 0.5$

(c) Group #3 $\frac{M_x}{M_x^{crit}} = 0.8$

Figure 7.7: Deformational patterns of elastic model for a_0=3 m at t=51s

The example of how deformational behavior of the riser in case of the heave amplitude a_0=3 m for three different torsion utilizations $\frac{M_x}{M_x^{crit}}$ at t=51s is provided in the Figure 7.7. From Figure 7.7a it can be noticed that, though the curvature in the activated length of the riser with torsion reaction utilization $\frac{M_x}{M_x^{crit}}$ of 0.25 is quite high, the kink is not formed (because of the fact that

κ_{t-max} is less than κ_{crit} at t=51s, see Figure 7.6a). In contrast to that, for the cases with torsion reaction utilizations $\frac{M_x}{M_x^{crit}}$ of 0.5 and 0.8 (when κ_{t-max} exceeds the limit of κ_{crit}), the kink is clearly established (see Figures 7.7b, 7.7c). Hence, this graphical visualization of the deformational patterns demonstrates that **the dynamic criterion** can be used as adequate methodology for kink formation prediction.

Overall, the following conclusions can be drawn from this parametric study:

1. *Torsion reaction utilization $\frac{M_x}{M_x^{crit}}$ and heave motion amplitude a_0 are both equally important for the physical process of kink formation.*

2. *The larger heave motion is, the bigger tension variation during the dynamic process is going to be. Hence, the increase in heave amplitude substantially influence the rise of the total curvature, which can lead to the kink formation.*

3. *Rise in the utilization of the torsion reaction (triggered by yaw motion of the vessel or local failure of tensile armor causing unbalanced rotation of tensile layers) can significantly increase the total curvature and, consequently, the chances for kink formation.*

7.5 Dynamic analysis of cyclic heave motion for COMPIPE42 model

In order to show the effect of non-linear material behavior on kink formation process during cyclic heave motion of the riser's end, the dynamic analysis is carried out for COMPIPE42 model, which is described in details in Chapter 6. It is important to remind a reader that the external diameter d_e of the cable for COMPIPE42 model is of 0.12m. Typically, for this value of external diameter the friction moment's M_f value for offshore power cables lies in the range between 0.81-1.0 kNm. Therefore, the value of M_f is chosen to be 0.85 kNm for all simulation cases described in this Section.

The load histories for the dynamic analysis of the COMPIPE42 model are almost the same as for elastic model case except for duration of the axial rotation imposition (instead of 20s as for elastic model, it is 40s). The applied load histories for COMPIPE42 model are provided below in the Table 7.2.

Time	Load description
0-5 s	Lifting the riser's end to the free surface (prescribed vertical displacement)
5-45 s	Imposed axial rotation in the top riser's end (prescribed axial rotation)
45-75 s	Cyclic heave motion of the top riser's end corresponding to Eq.(7.2)

Table 7.2: Load histories for dynamic analysis of COMPIPE42 model

The cyclic heave load histories of the top riser's end for different heave amplitudes a_0 are represented in the Figure 7.8.

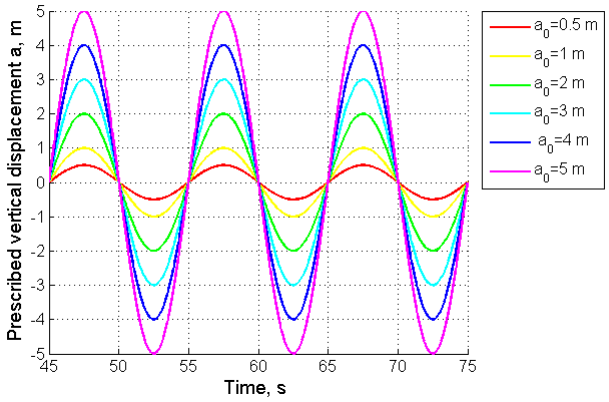

Figure 7.8: Cyclic heave load histories for dynamic analysis of COMPIPE42 model

7.6 Dynamic criterion. Parametric study for COMPIPE42 model

For application of **the dynamic criterion** for COMPIPE42 model the value of the critical total curvature κ_{crit} needs to be found for COMPIPE42 model . It is done exactly in the same way as for elastic model. Development of the maximum value of total curvature κ_{t-max} during utilization of the torsion reaction moment M_x is computed and shown in the Figure 7.9. From this

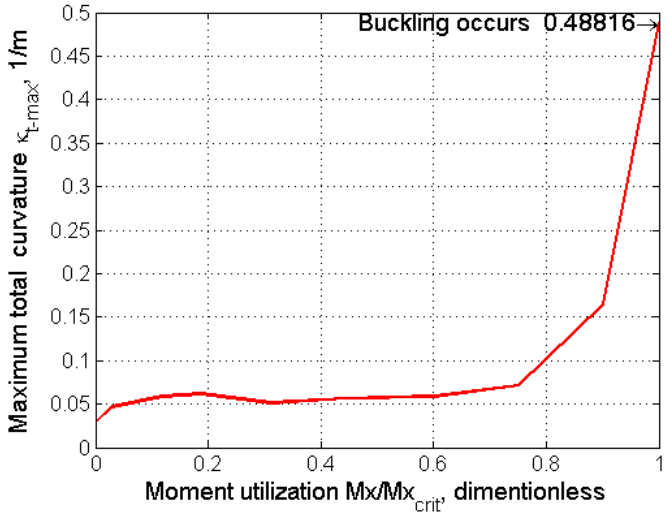

Figure 7.9: Development of the maximum value of total curvature for COMPIPE42 model

graph it can be clearly seen that the critical total curvature κ_{crit} is of 0.488 $\frac{1}{m}$. If, according to **the dynamic criterion**, the maximum value of the total curvature κ_{t-max} varying in time exceeds the κ_{crit} of 0.488 during the dynamic analysis of the heave motion, kink will be inevitably formed.

Parametric studies

As it is done previously for elastic model in the Section 7.4, the parametric study is also carried out for COMPIPE42 model with a purpose to evaluate applicability of **the dynamic criterion** for the model with non-linear material characteristics.

Numerous simulations performed for dynamic analysis of cyclic heave motion can be divided into five simulation groups, whose characteristics are provided in the Table 7.3:

Simulation group number	**Torsion reaction utilization** $\frac{M_x}{M_x^{crit}} \cdot 100\%$	**Imposed axial rotation in the top riser's end, rad**
#1	27%	13.4
#2	40%	20
#3	46%	23
#4	53.6%	26.8
#5	65.3%	33

Table 7.3: Simulation groups properties for dynamic analysis of the COMPIPE42 model

Each simulation group is subjected to cyclic heave loads with different amplitudes a_0 varying between 0.5m and 4m. The heave period T_h is kept to be constant of 10s. The results of the parametric study are presented for the first two circles of the heave load from 45s to 65s. (See Figure 7.10 on the next page).

The maximum value of the total curvature κ_{t-max} is monitored in time during cyclic heave motion for each simulation case. If this value of κ_{t-max} varying in time exceeds the critical total curvature κ_{crit} (depicted as a red dashed line in the Figure 7.10), that is a clear indication that kink is established.

The following conclusions can be made from this parametric study:

1. *Torsion reaction utilization* $\frac{M_x}{M_x^{crit}}$ *and heave motion amplitude* a_0 *both have the influence on* κ_{t-max}.

2. *The role of torsion reaction utilization in the kink formation process for COMPIPE42 model is much more crucial. For instance, having the torsion utilization of around 50% and higher, kink will be inevitably formed for any value of heave amplitude. This can be seen from the Figures 7.10d, 7.10e.*

3. *For high values of torsion reaction utilization, the influence of the heave amplitude on* κ_{t-max} *is negligible. See the example for the torsion utilization of 65.3% illustrated in the Figure 7.10e.*

4. *Comparing the results of this parametric study for COMPIPE42 model with the one of the parametric study for elastic model, one can find out that it is much more conservative for evaluation of kink formation to apply elastic model for lower utilizations of the torsion reactions. This is due to the fact that for elastic model high heave amplitude motion can*

cause kink formation even for the cases with small torsion utilizations. However, for larger values of $\frac{M_x}{M_x^{crit}}$ *(starting approximately from value of 0.5) it is more reasonable with respect to safety prospective to take into consideration COMPIPE42 model.*

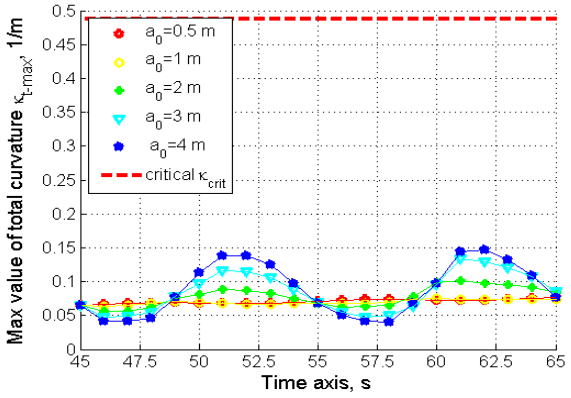

(a) Group #1 $\frac{M_x}{M_x^{crit}} = 0.27$

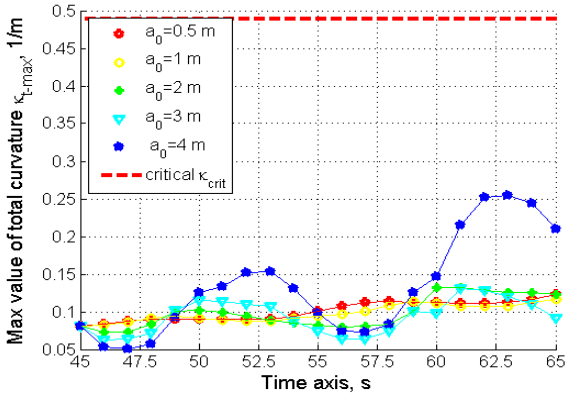

(b) Group #2 $\frac{M_x}{M_x^{crit}} = 0.4$

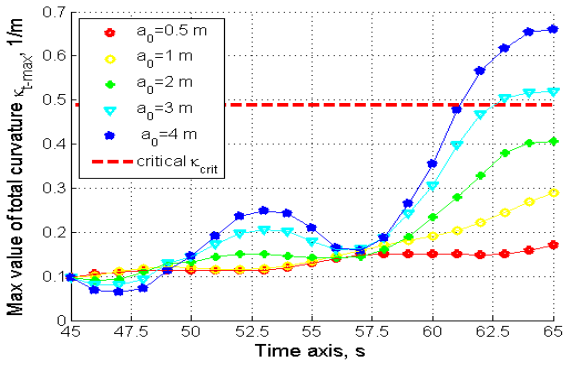

(c) Group #3 $\frac{M_x}{M_x^{crit}} = 0.46$

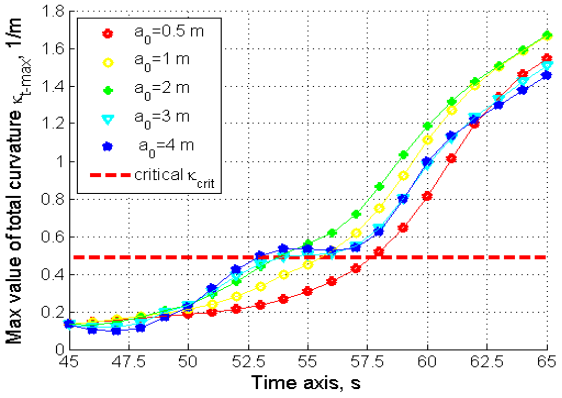

(d) Group #4 $\frac{M_x}{M_x^{crit}} = 0.536$

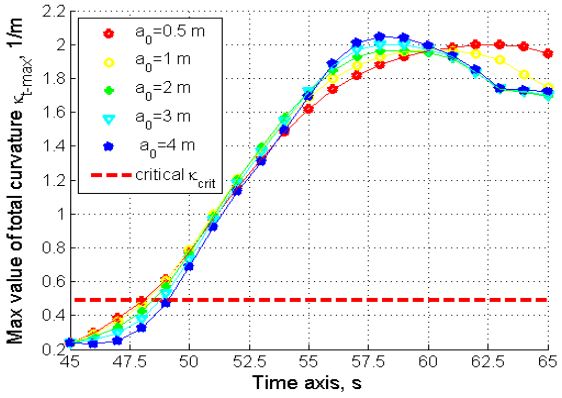

(e) Group #5 $\frac{M_x}{M_x^{crit}} = 0.653$

Figure 7.10: Development in time of the maximum value of total curvature for COMPIPE42 model

The examples of how deformational pattern of COMPIPE42 model when the kink is formed in case of the heave amplitude a_0=3 m for two different torsion utilizations $\frac{M_x}{M_x^{crit}}$ are illustrated in the Figure 7.11.

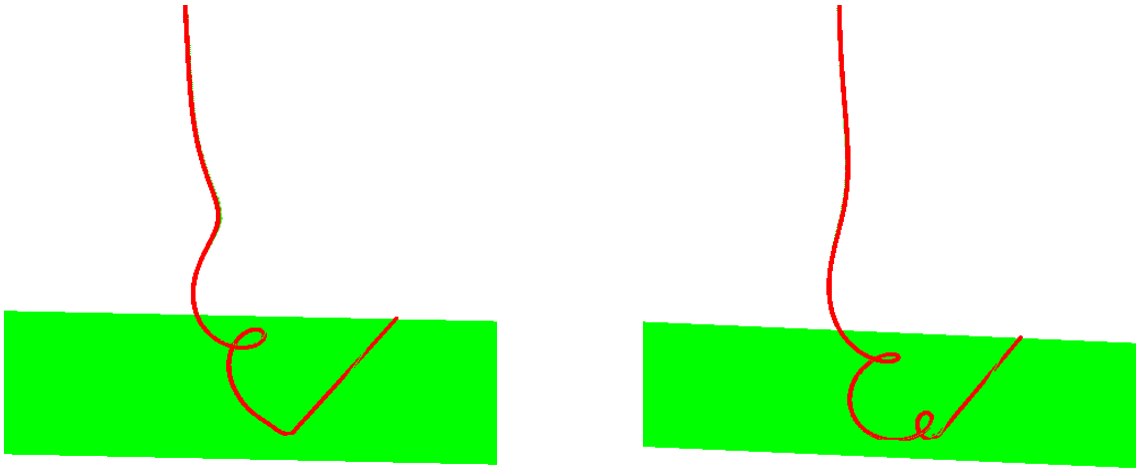

(a) Group #4 $\frac{M_x}{M_x^{crit}} = 0.536$ at 57s (b) Group #5 $\frac{M_x}{M_x^{crit}} = 0.653$ at 60s

Figure 7.11: Deformational patterns of COMPIPE42 model for a_0=3 m

7.7 Discussion about compression in the TDZ

Nowadays, in the offshore industry practice it is not allowed to have a compression in the TDZ at all. This quite conservative decision is made in order to avoid buckling failure modes in the TDZ. Consequently, the offshore companies very often suffer a lot due to this precaution, because they are forced to stop costly operations, if there is any chance that something (like weather conditions, etc) can cause compressive stresses in the TDP region.

However, with respect to torsion buckling failure modes this current industry practice can be argued. Let's look closely at the dynamic analyses of COMPIPE42 model performed for simulation group #1 of the parametric study in the previous Section 7.6. As it can be noticed from the Figure 7.10a, the riser with torsion reaction utilization $\frac{M_x}{M_x^{crit}}$ of 0.27 can be operated **without torsion failure** (even maintaining **significant safety margin)** for all applied heave amplitudes. Now, let's track how the tensile force along the riser's length in the TDZ varies during the first cycle of the heave motion from 45s to 55s. Figure 7.12 reveals that the higher heave motion

amplitude is applied, the larger tensile variation is going to happen. For the case with heave amplitude a_0 of 1 m represented in the Figure 7.12a the tensile variation is small and tension does not reach negative values. Hence, there is no compression in the TDZ for that case. However, for the other cases when a_0 is larger than 1m the tensile force along the riser's length in the TDZ varies between positive and negative values. Higher heave amplitude gives higher maximum compressive force (or minimum tensile force). The values of minimum tensile force are

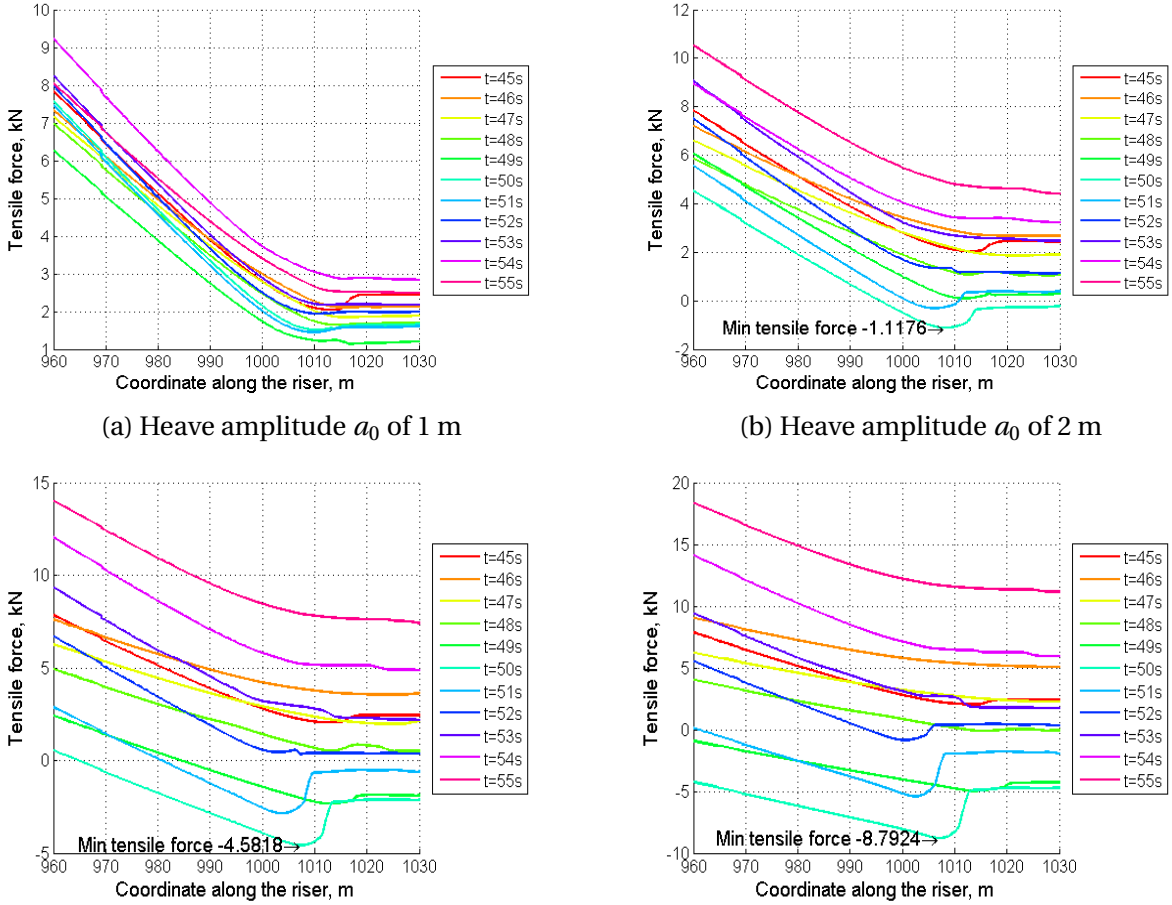

(a) Heave amplitude a_0 of 1 m

(b) Heave amplitude a_0 of 2 m

(c) Heave amplitude a_0 of 3 m

(d) Heave amplitude a_0 of 4 m

Figure 7.12: Tensile variation of the riser with $\frac{M_x}{M_x^{crit}}$ of 0.27 in the TDZ

found for each case and provided in the Figure 7.12.

Overall, very important conclusion with respect to practical standpoint can be drawn from this study and formulated in the following way: *In case of having utilized compression in the TDZ due to cyclic motion of the vessel , it is still possible for the structure to stay away from the torsion failure modes with substantial safety margin.*

Chapter 8

Concluding remarks

8.1 Conclusions

The main purpose of this thesis is to improve existing knowledge about torsion structural stability and kink formation process of flexible lines (risers/cables) in catenary configuration.

Before starting the investigation of the torsion buckling of flexible risers in catenary shape, the simplified elastic straight beam model with constant tension subjected to torsion load has been created in BFLEX2010 and tested with respect to torsion stability. The numerical result of critical torsion reaction moment computed by software shows excellent agreement with analytical solution calculated by using the Greenhill's formula.

In order to thoroughly explain the physical nature of the torsion buckling of catenary risers, definition of the activated length has been introduced. The knowledge about the limits of activated length gives an idea where kink can be possibly formed due to the transformation of torsion energy into bending energy.

Study cases performed for elastic PIPE31 model by means of BFLEX2010 showed that both: presence of the riser's tail resting on the seabed and the seabed friction can affect the critical torsion buckling moment and the deformational behavior of the system when the buckling occurs. Simulations carried out for this study demonstrate that at the moment when buckling occurs in case of having frictionless riser's tail on the seabed the tension in the TDZ is less than for the case of

having friction. Therefore, the critical torsion moment is smaller for the frictionless case, which from the engineering standpoint can be a good choice for prediction of the torsion buckling.

Another important outcome is that the Greenhill's analytical expression, which is valid for straight beam with constant tension, cannot give an adequate solution of critical torsion moment in case of catenary shaped riser. This is because of the fact that in catenary configuration the tensile force is not uniformly distributed along the riser's length from the sea surface down to the bottom. Additionally, tension increases in the activated length during the process of axial rotation utilization due to the transformation of the torsion energy into bending energy.

A special attention has been dedicated to the study of the impact of non-linear moment curvature behavior (sliding process between riser's layers) on the process of torsion buckling. It has been determined that torsion buckling capacity of the riser is significantly affected by the non-linear material characteristics. Parametric study carried out for COMPIPE42 model (representing non-linear material behavior) reveals that the critical torsion moment is directly proportional to the value of the friction moment. From another parametric study performed for non-linear COMPIPE42 model it has been determined that the influence of β parameter (governing the interaction between tensile and torsion strain components) on torsion buckling capacity is not substantial.

One of the most valuable and unique contribution of the thesis is that the dynamic criterion for evaluation of the kink formation for the catenary risers having initial torsion utilization and subjected to cyclic heave motion has been formulated and verified for the models with linearly elastic (PIPE31) and non-linear (COMPIPE42) material properties. Parametric studies conducted for these models show that torsion reaction utilization and heave motion amplitude are both equally important for the kink formation process in case of elastic model , while for the model with non-linear characteristics the role of amount of torsion utilization in the system is much more crucial. It has also been emphasized that from engineering standpoint it is much more conservative to apply elastic model for lower utilizations of the torsion reactions. However, the model with non-linear characteristics needs to be implemented for the cases with larger values of torsion reaction utilizations.

With respect to the point of view related to the current offshore industry practice, an important finding has been made that the structure can remain safe with respect to the torsion failure modes having compression utilized in the TDP region triggered by cyclic heave motion.

8.2 Recommendations for further work

It is recommended to conduct scale laboratory experiments with the purpose to reproduce elastic and non-linear riser models described in the thesis and investigate them with respect to torsion buckling capacity. Based on the experimental results the verdict about the numerical accuracy of BFLEX2010 can be delivered.

The influence of the interaction between tensile and torsion strain components (β parameter) on torsion buckling capacity has been found as a result of parametric study performed for COMPIPE42 model. Broadening this study, another parametric analysis can be performed with the purpose of taking into account the impact of radial strain components on torsion buckling behavior. In order to do so, appropriate model with HSHEAR363 element type has to be assembled.

Dynamic analysis of cyclic heave motion has been performed both for elastic and non-linear models (having utilized initial torsion reactions) with the intention of verification of the dynamic criterion for evaluation of kink formation. However, typically the motion of the laying vessel is much more complex compare to pure heave motion. Therefore, it is proposed to upgrade the motion of the vessel by taking into consideration sway, surge and heave components of the motion altogether.

The dynamic analyses for the non-linear model with respect to cyclic heave motion have been performed just for 3 cycles of load. From the Figure 7.10a it can be seen that with each cycle of load the plots follow slightly increasing trend. Therefore, there is a possibility that after high number of load cycles the structure will experience torsion failure. To verify that, dynamic analysis with a high cycled load history should be carried out.

It has been found that compression in the TDP region during the cyclic heave motion of the vessel can be up to 9kN and it does not cause torsion failure modes. However, this does not guarantee structural safety regarding local failure modes of tensile armor (lateral buckling and birdcaging). Therefore, local FEM analysis of tensile armor layers at the TDP needs to be a part of further work.

Appendix A

Input files

A.1 BFLEX2010 input file

The BFLEX2010 input file is provided below for the simplified beam model described in the Chapter 4. The rest of the BFLEX2010 input files for all analyses considered in the thesis can be found in the Digital Attachment enclosed to the thesis.

```
HEAD Simplified Beam model
#       MAX_ITER  NDIM ISOLVR NPOINT  IPRINT CONV_RAD  GRAV ISTRES
CONTROL  100       3    2      16       1      1e-5    9.81 stressfree
#Dynamic Analysis criteria
#         Lumped mass  alfa1  alfa2  HHT-alfa parameter
DYNCONT   1            0.0    0.051  -0.05
#Result visualization definition
VISRES integration 1 Vcondis-y vcondis-z vconfor-y sigma-xx vconfor-z
#     Mass    Length   Time
UNITS 1.0e-06   1        1

#GEOMETRY DATA
#============================================================================
#PIPE
#       type          NodeID    X     Y     Z
NOCOOR COORDINATES      1       0     0     0
REPEAT 101 1 1.0 0 0
#ELCON DATA for PIPE
```

```
ELCON   pipe1   pipe31  pipemat1 1 1 2
REPEAT 100 1 1

#-------------------------------------------------------------------------
# Orient input
#-------------------------------------------------------------------------
#pipe                   elno             x          y        z
ELORIENT COORDINATES       1             0.0     1.000      0.0
REPEAT 100 1 0 0 0
#ELEMENT DATA(PIPE DATA)
#      name  type rad   th   CDr Cdt CMr CMt wd        ws       ODp    ODw     rks
ELPROP pipe1 pipe 0.055 0.01 1.0 0.1 2.0 0.2 2.588e-5  1.43e-5   0.12    0.12   0.5
#BOUNDARY CONDITION
#=========================================================================
#        COSYS    NODEID    DOF
BONCON   GLOBAL      1        1
BONCON   GLOBAL      1        2
BONCON   GLOBAL      1        3
BONCON   GLOBAL      1        5
BONCON   GLOBAL      1        6
#
BONCON   GLOBAL      101        2
BONCON   GLOBAL      101        3
BONCON   GLOBAL      101        4
BONCON   GLOBAL      101        6
#LOAD INPUT
#External Pressure and Gravity Load
#       dmhist  b&pehist
PELOAD  100     100
CLOAD 150 1 101 98.64e-5
#PRESCRIBED DISPLACEMENT
CONSTR PDISP GLOBAL 1 4  3    400
#Analysis time control
#=========================================================================#
TIMECO      1.0   0.1     1.0  201.0  dynamic AUTO NONE ALL 100 2 1e-5
TIMECO      51.0  0.1     2.0  201.0  dynamic AUTO NONE ALL 100 2 1e-5
```

```
#TIMECO      80.0  1.0    70.0 201.0  dynamic AUTO GO-ON ALL 100 2 1e-5
#TIMECO      110.0 1.0    25.0 201.0  dynamic AUTO GO-ON ALL 100 2 1e-5
#-----------------------------------------------------------
# History data
#-----------------------------------------------------------
#     no     istp  fac buoyancy and external pressure
THIST 100    0.0    0.0
0.1    0.01
THIST 150 0.0   1.0
1.0   1.0
THIST_r 400 1.0 51.0 rampcos 1.0
#MATERIAL DATA
#-----------------------------------------------------------
#Main definition of the material type
#        name     type   poiss talfa tecond heatc beta ea   eiy    eiz        git em   gm
MATERIAL pipemat1 linear 0.3 1.17e-5 50     800   0    409.0 5.03e-3  5.03e-3  1  2e5 8e4
```

A.2 BFLEX2010POST input file

BFLEX2010POST input files are built in the same manner. The example of such input file is provided below.

```
#       raffile name       mpfpre xlab          Xleg      Xres     Yleg            yres fnodid lnodid  xscl yscl elend
glplot "dyn_3_comp"   "dyn_3_comp-ELMOMX-distr"  "S-cor (m)" e-cor "Elmom-x(kNm)"  elmom-x   1  2300    1   1e3  1
glplot "dyn_3_comp"   "dyn_3_comp-ELMOMY-distr"  "S-cor (m)" e-cor "Elmom-y(kNm)"  elmom-y   1  2300    1   1e3  1
glplot "dyn_3_comp"   "dyn_3_comp-ELMOMZ-distr"  "S-cor (m)" e-cor "Elmom-z(kNm)"  elmom-z   1  2300    1   1e3  1
glplot "dyn_3_comp"   "dyn_3_comp-ELforcex-distr""S-cor (m)" e-cor "Elfor-x(kNm)"  elforce-x 1  2300    1   1e3  1
glplot "dyn_3_comp"   "dyn_3_comp-ELCURZ-distr"  "S-cor (m)" e-cor "Elcur-z(1/m)"  elcur-z   1  2300    1   1  1
glplot "dyn_3_comp"   "dyn_3_comp-ELCURY-distr"  "S-cor (m)" e-cor "Elcur-y(1/m)"  elcur-y   1  2300    1   1  1
```

Appendix B

Matlab script

The example of BFLEX2010POST output data reading and plot generation is represented below. The result of this script execution is the creation of the Figure 6.8d.

```
clear all
close all
clc
%Mf=0.45kN
%% comp__10_45-ELMOMX-distr.mpf 31.00 sec
t33=50740;
t30=46128;
t31=48434;
t34=53046;
path='C:\Marintek\Bflex2010\4thsemester\bettastudy\betta10\'
fileID45 = fopen(fullfile(strcat(path,'comp__0_45-ELMOMX-distr.mpf')));
text45 = textscan(fileID45, '%s', 'Delimiter',' ', 'headerlines',t31);
text45{1};
text45{1}(:);
text45{1}(strcmp('',text45{1}(:))) = [];
a45 = text45{1}(2:end) ;
dim = length(a45) / 2;
%format bank
d45 = str2double(a45) ;
x45 = d45(1:2:4600);
y45 = d45(2:2:4600);
```

```
meany45=mean(y45)
% f45=figure;
% plot (x45,y45)
% %  ylim([13 14])
%   xlim([0 1600])
% x45;
% y45;
%% comp__10_20-ELMOMX-distr.mpf 31.00 sec
t33=50740;
t30=46128;
t31=48434;
t34=53046;
path='C:\Marintek\Bflex2010\4thsemester\bettastudy\betta10\'
fileID20 = fopen(fullfile(strcat(path,'comp__0_20-ELMOMX-distr.mpf')));
text20 = textscan(fileID20, '%s', 'Delimiter',' ', 'headerlines',t31);
text20{1};
text20{1}(:);
text20{1}(strcmp('',text20{1}(:))) = [];
a20 = text20{1}(2:end) ;
dim = length(a20) / 2;
%format bank
d20 = str2double(a20) ;
x20 = d20(1:2:4600);
y20 = d20(2:2:4600);
meany20=mean(y20)
% f20=figure;
% plot (x20,y20)
% %  ylim([13 14])
%   xlim([0 1600])
% x20;
% y20;
%% comp__10_100-ELMOMX-distr.mpf 31.00 sec
t33=50740;
t30=46128;
t31=48434;
t34=53046;
```

```
path='C:\Marintek\Bflex2010\4thsemester\bettastudy\betta10\'
fileID100 = fopen(fullfile(strcat(path,'comp__0_100-ELMOMX-distr.mpf')));
text100 = textscan(fileID100, '%s', 'Delimiter',' ', 'headerlines',t31);
text100{1};
text100{1}(:);
text100{1}(strcmp('',text100{1}(:))) = [];
a100 = text100{1}(2:end) ;
dim = length(a100) / 2;
%format bank
d100 = str2double(a100) ;
x100 = d100(1:2:4600);
y100 = d100(2:2:4600);
meany100=mean(y100)
% f100=figure;
% plot (x100,y100)
% %  ylim([13 14])
%   xlim([0 1600])
% x100;
% y100;
%%
path='C:\studies\4semester\thesis\';
fid = fopen(fullfile(strcat(path,'compipe_criticalmoments.txt')));
C = textscan(fid, '%s','delimiter', '\n');
Mt0=C{1}{14};
Mt0_1 = str2double(Mt0) ;
beta=0:0.01:0.03;
Mt= [Mt0_1 meany100 meany20 meany45]
f1=figure;
l=length(beta);
cc=hsv(l); %colormaps hsv ,jet
hold on ;
for i=1:l;
plot(beta(i),Mt(i),'o' ,'color',cc(i,:),'Linewidth',3.5);
end
% plot (beta,Mt,'o');
xlabel('\beta, m', 'FontSize', 15);
```

```
ylabel('Critical Torsion Moment, kNm', 'FontSize', 14);
legend('\beta=0.00 m','\beta=0.01 m','\beta=0.02 m','\beta=0.03 m','Location','northeast');
set(gca,'FontSize',12);
hold on;
p=polyfit(beta,Mt,3);
plot(beta,polyval(p,beta),'r');
grid on;
figuresdir = 'C:\studies\4semester\thesisEKlatex\fig\';
hgexport(gcf, strcat(figuresdir, 'betacomp0'), hgexport('factorystyle'), 'Format', 'png');
```

Bibliography

[1] 4SubseaAS (2013). *Un-bonded Flexible Risers – Recent Field Experience and Actions for Increased Robustness.*

[2] API17B (2002). *Recommended Practice for flexible pipes.*

[3] API17J (2008). *Recommended Practice for flexible pipes.*

[4] Bai, Y. (2003). *Pipelines and Risers.* ELSEVIER SCIENCE Ltd.

[5] Bazant, Z. and Cedolin, L. (2010). *Stability of Structures. Elastic, Inelastic, Fracture and Damage Theories.* World Scientific Publishing Co.

[6] Bell, K. *An engineering approach to Finite Element Analysis of linear structural mechanical problems.* Fagbokforlaget, Bergen.

[7] Berge, S., Engseth, A., Fylling, I., Larsen, C., Leira, B., Nygaard, I., and Olufesn, A. Handbook on design and operation of flexible pipes. Technical report, NTNU, 4Subsea and MARINTEK.

[8] Liu, F. Kink formation and rotational response of single and multistrand electromechanical cables. Technical report, CIVIL ENGINEERING LABORATORY, Naval Construction Battalion Center.

[9] Lundteigen, M. A. and Rausand, M. (2008). Spurious activation of safety instrumented systems in the oil and gas industry: Basic concepts and formulas. *Reliability Engineering and System Safety*, 93:1208–1217.

[10] Moan, T. (2003). Finite element modeling and analysis of marine structures.

[11] Neto, A. and Martins, C. (2013). Structural stability of flexible lines in catenary configuration under torsion. *Marine Structures*, 34:16–40.

[12] Rausand, M. (2014). *Reiability of Safety-Critical Systems: Theory and Applications*. Wiley, Hoboken, NJ.

[13] Rausand, M. and Høyland, A. (2004). *System Reliability Theory: Models, Statistical Methods, and Applications*. Wiley, Hoboken, NJ, 2nd edition.

[14] Østergaard, N., Lyckegaard, A., and Andreasen, J. (2012a). Imperfection analysis of flexible pipe armor wires in compression and bending. *Applied Ocean Research*, pages 40–47.

[15] Østergaard, N., Lyckegaard, A., and Andreasen, J. (2012b). On modeling of lateral buckling failure in flexible pipe. *Marine Structures*, pages 64–81.

[16] Sævik, S. Bflex2010-theory manual. Technical report, NTNU, MARINTEK.

[17] Sævik, S. (1992). On stresses and fatigue in flexible pipes.

[18] Sævik, S. (2011). Theoretical and experimental studies of stress in flexible pipe. *Computers and Structures*, pages 2273–2291.

[19] Sævik, S. (2015). Lecture notes in offshore pipeline technology.

[20] Sævik, S., Økland, O., Baarholm, G., and K., G. Bflex2010 version 3.0.9 user manual. Technical report, NTNU, MARINTEK.